UNIVERSITY OF CALIFORNIA, SAN DIEGO

Major Histocompatibility Complex Class I is a Negative Regulator of Neuronal Insulin Receptor Signaling and Hippocampal Synapse Number

A dissertation submitted in partial satisfaction of the
requirements for the degree Doctor of Philosophy

in

Biology

by

Tracy Jean Dixon Salazar

Committee in charge:

Professor Lisa Boulanger, Chair
Professor Joseph Gleeson
Professor Steve Hedrick
Professor Gentry Patrick
Professor Yimin Zou

2009

The Dissertation of Tracy Jean Dixon Salazar is approved, and it is acceptable in quality and form for publication on microfilm and electronically:

_____

_____

_____

_____

_____

Chair

University of California, San Diego

2009

DEDICATION

This work is dedicated to my amazing family. You are my sun.

EPIGRAPH

Each generation of scientists stands upon the shoulders of those who have gone before.

Owen Chamberlain

TABLE OF CONTENTS

LIST OF ABBREVIATIONS

β2m	Beta-2-microglobulin
BSA	Bovine Serum Albumin
CNS	Central Nervous System
DIV	Days *in vitro*
GFP	Green Fluorescent Protein
IGF-1R	Insulin-like Growth Factor-1 Receptor
IR	Insulin Receptor(s)
MHCI	Major Histocompatibility Complex Class I
O/N	Overnight
PBS	Phosphate Buffered Saline
PFA	Paraformaldehyde
PI3K	Phosphoinositide 3-kinase
PirB	Paired Immunoglobulin-like Receptor B
RT	Room Temperature
SEM	Standard Error of the Mean
TAP	Transporter Associated with Antigen Processing 1
WT	Wild-type

LIST OF FIGURES

ACKNOWLEGEMENTS

I would like to acknowledge Professor Lisa Boulanger for her support as my thesis advisor and chair of my committee. Through multiple drafts and many longs nights, her guidance has proved invaluable.

I would also like to acknowledge my thesis committee, Joe Gleeson, Steve Hedrick, Gentry Patrick and Yimin Zou. Thank you for your sharp minds, keen guidance and never-ending support.

Chapters 3 and 4, in part, have been submitted for publication of the material as it may appear in Neuron, 2010, Dixon-Salazar, Tracy; Fourgeaud, Lawrence; Boulanger, Lisa, Cell Press, 2010. The dissertation author was the primary investigator and author of this paper.

VITA

2000-2002	Teaching Assistant, Grossmont College, El Cajon
2001	Associate of Science, with honors, Grossmont College, El Cajon
2002-2004	Research Assistant, University of California, San Diego
2004	Bachelor of Science, *cum laude,* University of California, San Diego
2006-2008	Teaching Assistant, University of California, San Diego
2009	Doctor of Philosophy, University of California, San Diego

PUBLICATIONS

Dixon-Salazar TJ, Keeler LC, Trauner DA, Gleeson JG, Autism in Several Affected Members of a GEFS^{+} Family. *J Child Neurol*. 2004 Aug;19(8):597-603.

Dixon-Salazar TJ, Silhavy JL, Marsh SE, Louie CM, Scott LC, Gururaj A, Al-Gazali L, Al-Tawari AA, Kayserili H, Sztriha L, Gleeson JG. Mutations in the *AHI1* Gene Encoding Jouberin, cause Joubert Syndrome with Cortical Polymicrogyria. *Am J Hum Genet*. 2004 Dec;75(6):979-87.

Valente EM, Marsh SE, Castori M, **Dixon-Salazar TJ**, Bertinin E, Al-Gazali L, Messer J, Barbot C, Woods CG, Boltshauser E, Al-Tawari AA, Salpietro CD, Kayserili H, Sztriha L, Gribaa M, Koenig M, Dallapiccola B, Gleeson JG. Distinguishing the four genetic causes of Joubert syndrome-related disorders. *Ann Neurol.* 2005 Apr;57(4):513-19.

Dixon-Salazar TJ, Fourgeaud L, Boulanger, LM. Regulation of insulin receptor phosphorylation and synapse number by MHC class I. *Neuron.* 2010. In revision.

FIELDS OF STUDY

Major Field: Neurobiology

Studies in Cellular Neurobiology and Biochemistry	Professor Lisa Boulanger
Studies in Neuronal Electrophysiology	Professor Dan Feldman
Studies in Cellular and Molecular Neurobiology	Professor Anirvan Ghosh

ABSTRACT OF THE DISSERTATION

Major Histocompatibility Complex Class I is a Negative Regulator of Neuronal Insulin Receptor Signaling and Hippocampal Synapse Number

by

Tracy Jean Dixon Salazar

Doctor of Philosophy in Biology

University of California, San Diego, 2009

Professor Lisa Boulanger, Chair

Major Histocompatibility Complex Class I (MHCI) proteins were first identified in the immune system but are also expressed in neurons and play a role in normal brain development and plasticity. However little is known about how, on a molecular level, MHCI modifies neuronal structure and function. Here we show that MHCI proteins

interact with neuronal insulin receptors (IR) and are critical for their signaling. Dendritically expressed MHCI is closely apposed to axonally expressed IR in many brain regions, including hippocampus, and MHCI co-immunoprecipitates with IR from mouse hippocampal lysates. Unexpectedly, genetic reduction of cell surface MHCI in either $\beta 2m^{-/-}TAP^{-/-}$ or $K^{b-/-}D^{b-/-}$ mice selectively alters antibody binding to an intracellular domain of the β-subunit of IR, which contains key tyrosine residues that are autophosphorylated following ligand binding. This loss of antibody binding can be rescued by co-culturing $\beta 2m^{-/-}TAP^{-/-}$ neurons with wild-type neurons, suggesting MHCI and IR can interact in *trans*. Furthermore, $\beta 2m^{-/-}TAP^{-/-}$ mice show an increase in basal tyrosine phosphorylation of IR. This increase in basal activation of IR correlates with an increase in synapse density in MHCI-deficient animals specifically in regions where IR are expressed. Together our results demonstrate that endogenous MHCI is a novel regulator of neuronal IR function and synapse number, and suggest that MHCI modifies a key c-terminal signaling domain of IR in neurons.

1 INTRODUCTION

1.1. The Major Histocompatibility Complex Class I (MHCI)

The constellation of genes found on the short arm of human chromosome 6 is collectively known as the Major Histocompatibility Complex Class I (MHCI). The MHCI gene region spans approximately 2 Mega-bases (Mb) and consists of 3 classical MHCI genes, 16 non-classical MHCI genes and 7 MHCI-like genes. The MHCI gene region is highly polymorphic and over 50 alleles have been observed for some MHCI family members. Most MHCI genes code for single-pass transmembrane proteins with large extracellular globular domains and small cytoplasmic tails, and MHCI proteins are expressed by most cells of the body (Horton et al., 2004; Milner and Campbell, 1992; Rhodes and Trowsdale, 1999; Weiss et al., 1984).

MHCI proteins play a key role in the immune system where they act in the process of antigen presentation in the adaptive immune system. In the adaptive immune response, surface-expressed MHCI proteins present intracellularly-derived peptide fragments, also known as antigens, to surveying immune cells. The peptides presented can be self (originate from the cell itself), or non-self (originate from an invading pathogen) and cells presenting non-self peptides are subsequently destroyed. This function of MHCI, termed antigen presentation, is the primary way they body rids itself of infected, transplanted and cancerous cells (Monaco, 1992; Neefjes and Momburg, 1993; Rammensee et al., 1993; Shawar et al., 1994).

In addition to its well-known immune roles, accumulating evidence indicates that MHCI has unexpected, non-immune functions in the developing and adult CNS. MHCI mRNA and protein are broadly expressed in normal, healthy neurons (Goddard et al.,

2007; Huh et al., 2000; Lidman et al., 1999; Linda et al., 1999; Zhong et al., 2006). Further, cell surface MHCI expression is required for normal synapse elimination in the developing retinogeniculate projection and normal synaptic plasticity in the adult hippocampus (Goddard et al., 2007; Huh et al., 2000; Oliveira et al., 2004). Since most, if not all, of the known functions of MHCI require interactions with other proteins, a critical first step in elucidating the molecular mechanisms of MHCI signaling in the brain is to identify its neuronal binding partners.

Recent studies have identified an immunoreceptor, Paired Immunoglobulin-like Receptor B (PirB), which is expressed by neurons and can bind to MHCI in neuronal culture preparations (Syken et al., 2006). Mice expressing a truncated, function-blocking form of PirB, however, do not mimic the failure of retinogeniculate synapse elimination seen in MHCI deficient animals, suggesting that MHCI may bind to additional, and as yet unidentified, neuronal cell surface receptors. Indeed, MHCI proteins are known to bind to dozens of immunoreceptors in non-neuronal cells (Bennett et al., 2000; Boyington and Sun, 2002; Held and Mariuzza, 2008; Ojcius et al., 2002). Therefore, it is possible that MHCI may mediate its non-immune effects in the brain by binding to immunoreceptors, or alternatively, to neuronal proteins that have no known immune function.

1.2. Insulin Receptor/Insulin Receptors (IR)

Insulin Receptor/Insulin Receptors (IR) are expressed on the surface of many cell types, including liver, muscle and fat cells, and are members of the Receptor Tyrosine Kinase protein family. IR bind with high affinity to circulating insulin via their extracellular insulin-binding domains. Insulin binding leads to a conformational change

in the intracellular portion of IR such that both the tyrosine kinase domain and several tyrosine residues become exposed. The exposed tyrosines are immediately autophosphorylated by the kinase domain, and this leads to the subsequent recruitment and activation of downstream second messengers. The activation of IR can initiate numerous intracellular second messenger signaling cascades and signaling of IR is known to play a role in cell growth, metabolism and survival (Shpakov and Pertseva, 2000; Ullrich and Schlessinger, 1990; Van Horn et al., 1994; Van Obberghen et al., 1985; White and Kahn, 1994).

Outside the brain, IR are best known for their role in regulating cellular glucose metabolism. In this process of energy metabolism, food intake leads to an increase in blood glucose levels and this is followed by the release of insulin, from the pancreas, into the bloodstream. Insulin binding to IR on the cell surface initiates an intracellular signaling cascade that leads to the upregulation of glucose transporters by the cell. These transporters allow for the transfer of circulating glucose into the cell body where it can then be metabolized to create energy for cellular processes. This transfer results in a consequent decrease in circulating blood glucose levels. A defect in the ability of IR to bind insulin results in insulin insensitivity and is the main pathogenic mechanism underlying Diabetes Mellitus Type II (De Meyts and Whittaker, 2002; McInnes and Sykes, 1997; Ward and Lawrence, 2009).

Inside the brain, neurons take up glucose primarily via insulin-independent mechanisms, suggesting that IR play a unique role in neuronal tissue (Plum et al., 2005; Schulingkamp et al., 2000; Tomlinson and Gardiner, 2008). Instead, neuronal IR have been implicated in numerous processes including control of feeding behavior, regulation

of reproduction and determination of lifespan (Bruning et al., 2000; Russell and Kahn, 2007; Tatar et al., 2001). During brain development, signaling by IR also determines synapse number in the developing *Xenopus* optic tectum (Chiu et al., 2008). Additionally, insulin – which is readily transported into the CNS and binds to either IR or insulin growth factor 1 receptors (IGF-1R) – can modify the trafficking of excitatory and inhibitory neurotransmitter receptors (Beattie et al., 2000; Lin et al., 2000; Man et al., 2000; Passafaro et al., 2001; Skeberdis et al., 2001; Wan et al., 1997), can alter synaptic plasticity (Ahmadian et al., 2004; Huang et al., 2003; van der Heide et al., 2005) and acts in learning and memory (Benedict et al., 2006; Tomioka et al., 2006; Zhao et al., 1999). Given that IR and MHCI are both expressed in the developing and adult brain and act in circuit formation and synaptic plasticity, it is plausible to hypothesize that these two proteins act in concert in these processes.

1.3. Evidence for an interaction between MHCI and IR outside the brain

Experiments in non-neuronal cell types suggest that MHCI may interact with IR. Fluorescence Resonance Energy Transfer (FRET) and co-immunoprecipitation experiments show that MHCI proteins are associated with IR in lymphocytes, adipocytes and liver plasma membranes (Chvatchko et al., 1983; Due et al., 1986; Edidin and Reiland, 1990; Phillips et al., 1986; Samson et al., 1986; Verland et al., 1989). Furthermore, lymphocytes expressing reduced levels of MHCI show defects in insulin-stimulated trafficking of IR (Assa-Kunik et al., 2003; Liegler et al., 1991). Moreover, peptide fragments derived from the α1 helix of classical MHCI molecules bind to IR and can enhance insulin-stimulated glucose uptake by cells (Hansen et al., 1989; Olsson et al.,

1994; Stagsted et al., 1993; Stagsted et al., 1990). Thus, in lymphocytes, adipocytes and hepatocytes, MHCI may interact with IR, and disruption of this interaction may affect the function of IR. Whether MHCI and IR interact in neurons, however, has not been explored, and the cellular and molecular effects of such an interaction have not been determined.

1.4. Aims of the study and major findings

To test whether MHCI and IR interact in neurons, expression and signaling of IR was examined in neurons from wild-type (WT) and MHCI-deficient ($\beta 2m^{-/-}TAP^{-/-}$ and $K^{b-/-}D^{b-/-}$) mice. IR are expressed broadly in WT mouse brain including cortex, hippocampus and cerebellum. IR are detected in close apposition to MHCI-positive puncta in neurons and MHCI and IR co-precipitate from hippocampal homogenates suggesting these proteins interact in the brain. Strikingly, in $\beta 2m^{-/-}TAP^{-/-}$ brains, immunostaining with an antibody against the c-terminal domain of the β-subunit of IR is completely abolished. Immunolabeling of IR is also significantly attenuated in $K^{b-/-}D^{b-/-}$ mice. Antibody- and fluorescent insulin binding studies, together with biochemical detection of denatured IR, suggest that the loss of immunostaining of IR in MHCI-deficient brains is due to a selective MHCI-dependent masking of a c-terminal epitope of the β-subunit of IR. The putative masked epitope encompasses tyrosine residues that are autophosphorylated at the start of insulin-induced signaling by IR, raising the possibility that MHCI may affect the activation of neuronal IR. Indeed, phosphorylation of IR is tonically elevated in $\beta 2m^{-/-}TAP^{-/-}$ neurons, and insulin treatment fails to promote further phosphorylation of IR. Previous studies suggest that signaling by neuronal IR enhances synapse number, and

consistent with this, synapse number is increased in $\beta 2m^{-/-}TAP^{-/-}$ and $K^{b-/-}D^{b-/-}$ mice selectively in regions where IR are expressed. Together these data provide the first evidence that MHCI regulates the activation of neuronal IR, and suggest MHCI may limit synapse number by preventing constitutive tyrosine phosphorylation of IR in the absence of ligand. More broadly, these results demonstrate that neuronal MHCI can affect brain circuitry by modifying the function of a non-immune receptor. Thus, they suggest that the neuronal functions of MHCI are in some cases mediated through novel, non-immune mechanisms.

2 MATERIALS AND METHODS

2.1. Animals and transgenic lines

All animal work was done in accordance with the University of California, San Diego Animal Subjects Program. WT C57Bl/6 mice and WT actin-GFP, $\beta 2m^{-/-}TAP^{-/-}$ and $K^{b-/-}D^{b-/-}$mice (kindly provided by A. Ghosh, D. Raulet/C.Shatz and H. Pleogh respectively) on a C57Bl/6 background, backcrossed to WT >8 times, were used in these studies. All mice were male, aged postnatal day 30-32 (P30-P32) unless otherwise specified. To reduce cell surface expression of most of the over 50 MHCI proteins found in mouse, we used $\beta 2m^{-/-}TAP^{-/-}$ animals. These mice lack two key components of the MHCI expression pathway: β2-microglobulin (β2m), an invariant light chain of the MHCI complex, and the transporter associated with antigen processing-1 (TAP), an endoplasmic reticulum expressed transporter required to load antigenic peptides onto MHCI. Double mutant $\beta 2m^{-/-}TAP^{-/-}$ mice lack stable cell surface expression of most members of the MHCI proteins, and have been used extensively to study the immunological functions of this protein family (Ljunggren et al., 1995; Van Kaer et al., 1992; Zijlstra et al., 1989). $K^{b-/-}D^{b-/-}$mice lack expression of the two so-called classical MHCI genes in C57BL/6 mice, H2-K and H2-D. Classical MHCI proteins are known for their role in antigen presentation and T-cell activation (Schott et al., 2003; Vugmeyster et al., 1998). WT actin-GFP mice express the GFP transgene under the control of the β-actin promoter (Okabe et al., 1997; Polleux and Ghosh, 2002) and therefore express GFP in all their neurons.

2.2. Immunostaining

For immunohistochemistry, mice were perfused with 1X phosphate buffered saline (PBS) at 37˚C, followed by 4% paraformaldehyde (PFA) at room temperature (RT). Brains were dissected out and post-fixed for 3 hours in PFA, then cryoprotected for overnight (O/N) in 10% O/N, then 20% O/N, then 30% O/N sucrose/1X PBS (Sigma). Brains were then frozen at -20C in optimal cutting temperature (OCT) gel and cryostat sectioned (20μm). Sections were mounted on Superfrost Plus Slides (Fisher) and allowed to air dry for 2 hours. Slides were washed once in PBS, blocked for 1 hour in 3% bovine serum albumin (BSA) + 0.3% Triton-X in PBS at RT unless otherwise specified. Slides were then incubated O/N at 4°C in primary antibodies against the protein of interest: IRβ (C19, 2μg/mL, Santa Cruz), MAP2 (MAB378, 1μg/mL, Chemicon), TAU (MAB3420, 1μg/mL, Chemicon), MHCI (OX18, MCA51R, 10μg/mL, Serotec, no Triton-X used), Calbindin (D-28K, C9848, 14μg/mL, Sigma, block in 2% goat serum). Purified isotype-matched IgG (R&D) was used in the same quantity as primary antibody as a negative control. After 3 brief washes in PBS, slides were incubated in secondary antibody (Alexa Fluor 488 or 568 IgG, 2μg/mL, Invitrogen) for 2 hours at RT in the dark. Following 5 brief washes in PBS and 3 hours of air drying at RT, slides were coverslipped using Gel Mount (Sigma).

For antigen retrieval, brain sections were incubated in a high pH urea buffer at 95°C for 10 minutes prior to blocking, then processed for IRβ (C19) immunostaining using the same procedure above.

For immunocytochemistry, hippocampal neurons in culture (see below; 16-20 days in vitro, DIV) were fixed in 4% PFA/4% sucrose for 15 min at RT followed by quenching in 100mM Glycine-PBS for 10 min to block free aldehyde groups that remain

after fixation. Coverslips were blocked in 0.2% BSA + 0.05% Saponin in PBS for 45 min at 37°C, then incubated 45 min at RT in primary antibody against the protein of interest dissolved in blocking solution: IRβ (C19, 2μg/mL), Calbindin (D-28K, 74μg/mL), IRβ (RTK, 611276, 5μg/mL, BD Transduction Labs), IRβ (D17, 2μg/mL, Santa Cruz), IRα (N20, 2μg/mL, Santa Cruz), GFP (ab6673, 0.3μg/mL, Abcam). Coverslips were washed briefly 4 times in PBS, incubated in secondary antibody (Alexa Fluor 488 or 568 IgG, 2μg/mL) in PBS 45 min at RT and briefly washed 5 times each in BSA-Saponin-PBS, then BSA-PBS, then PBS alone. Coverslips were mounted to slides with Gel Mount.

All experiments were visualized using standard fluorescent microscopy using an Olympus BX51W upright microscope. All within-experiment comparisons were made from samples prepared from mice of the same genotype, age and sex, perfused on the same day, processed under the same conditions, mounted on the same slide and visualized using the same parameters. For double labeling experiments, neurons were incubated in both antibodies simultaneously. For confocal microscopy, all images were taken with a Leica DMI6000 inverted microscope outfitted with a Yokogawa Nipkon spinning disk confocal head, an Orca ER high resolution B&W cooled CCD camera (6.45 μm/pixel at 1X), Plan Apochromat 40X/1.25na and 63X/1.4na objective, and an argon/krypton 100mW air-cooled laser for 488/568/647 nm excitations. All images were acquired in the dynamic range of 8 bit or 12 bit acquisition. Maximum projected confocal Z-stacks were analyzed with National Institutes of Health (NIH) ImageJ.

2.3. Western blot

To prepare tissue for blotting, mice were briefly anesthetized with Isoflurane followed by rapid decapitation. Hippocampi were dissected out in ice cold 1X PBS and homogenized with a handheld tissue grinder in lysis buffer [20mM Tris (pH 7.5), 1mM EDTA (pH 8), 150mM NaCl, 1% NP40, and protease (Complete Tabs) and phosphatase (PhosStop) inhibitor cocktails (Roche)]. After 30 min of incubation on ice, samples were centrifuged to remove insoluble material. Protein quantification was performed using a BCA protein assay kit (Pierce). Samples (50-500μg) were heat denatured in 2X sodium dodecyl sulfate (SDS) sample buffer/lysis buffer [125mM Tris (pH 6.8), 4% SDS, 10% glycerol, 0.006% bromophenol blue, 1.8% β-mercaptoethanol] at 85°C for 5 min and run on using standard SDS-PAGE. Proteins were then transferred to a PVDF membrane (Millipore) in methanol-containing transfer buffer. Membranes were blocked in 5% milk/1X TBS/0.1% Tween, then probed with primary antibody against the proteins of interest: IRβ (C19, 200μg/mL), MHCI (OX18, 1mg/mL), GluR1 (AB1504, 100μg/mL, Chemicon), GAPDH (MAB374, 10μg/mL, Chemicon), Synaptophysin (MAB5258, 10μg/mL, Chemicon) or pTyr (4G10, 0.5μg/mL, Upstate, block 2% BSA instead of milk). After 5 brief washes in milk, membranes were incubated for 1 hour in secondary antibody dissolved in milk (Peroxidase-conjugated AffiniPure IgG, 0.1-0.2μg/mL, Jackson). Bands were visualized using a chemiluminescent detectant (Pierce) and quantified by densiometry using Image J Software (NIH).

For insulin treatment of live hippocampal slices, coronal brain slices (350μm thick) were cut in artificial cerebrospinal fluid (ACSF; containing in mM: 117 NaCl, 4.7 KCl, 25 $NaHCO_3$, 1.2 NaH_2PO_4, 11 Dextrose, 2.5 $CaCl_2$, 1.2 $MgCl_2$) and allowed to recover 30 min in oxygenated ACSF at 31°C, followed by 30 min at RT. These slice

preparations are routinely used in the lab for electrophysiological recordings. Half the sections from one animal were treated for 30 min with 1.5μM bovine insulin (Sigma, I0516) in 25mM HEPES, while the other half were treated with HEPES only. Hippocampi were then dissected out and processed for western blot or immunostaining as above or immunoprecipitation as below.

2.4. Immunoprecipitation

Insulin-treated, vehicle-treated or untreated hippocampal protein lysates (1mg) were incubated O/N at 4°C with 2μg of precipitating antibody. Samples were combined with 50μL of prewashed Protein G beads (Promega) in lysis buffer and rotated for 3 hours at 4°C. Beads were collected by centrifugation and washed 3 times in cold lysis buffer. Immunoprecipitates were eluted directly in SDS sample buffer at 85°C for 10 min. Immunoprecipitates were analyzed by western blot as above.

2.5. Surface biotinylation

To examine surface proteins, dissected hippocampi were immediately washed in ice-cold ACSF and incubated in ACSF containing 1mg/mL sulfosuccinimidyl-6-(biotinamido) hexanoate (Pierce) for 1 hour at 4°C. Unreacted biotinylation reagent was removed by two 10 min washes in ice-cold ACSF, and quenched with two 20 min washes in ice-cold ACSF plus 100mM glycine. Hippocampi were then homogenized as described above. To pull down biotinylated proteins, 250μg of each lysate was incubated with 50μL of streptavidin agarose beads (Endogen) O/N at 4°C. After 4 washes in lysis

buffer and one in 50mM Tris-HCl (pH 7.4), surface proteins were eluted into SDS sample buffer. Biotinylated proteins were analyzed by western blot.

2.6. Subcellular fractionation

For each experiment, two sex-matched 4- to 5-week-old animals from each genotype (WT and *β2m*$^{-/-}$*TAP*$^{-/-}$) were used. Briefly, brains were quickly removed, hippocampi dissected out and homogenized in 10 volumes of HEPES sucrose buffer [0.32 M sucrose, 4 mM HEPES (pH 7.4) supplemented with anti protease inhibitor cocktail (Complete, Roche) using a glass-teflon homogenizer at 900rpm (12 strokes). The homogenate was centrifuged 10 min at 1000xg. The pellet (P1), containing the nuclei and large insoluble fragments, was discarded. The supernatant (S1), corresponding to the total protein fraction, was centrifuged 20 min at 10000xg resulting in a crude synaptosomal pellet (P2). P2 was resuspended in 10 volumes of HEPES sucrose buffer and centrifuged again for 10 min at 20000xg, resulting in a washed crude synaptosomal pellet (P2'). P2' was subsequently lysed by hypo-osmotic shock in water and rapidly adjusted to 4mM HEPES. After a 30 min rotation at 4°C, the P2' lysate was centrifuged 20 min at 25000xg, resulting in a crude synaptosomal membrane fraction (P3) and a crude synaptic vesicle fraction (S3). Small aliquots were collected at all steps of the fractionation and solubilized by addition of triton (1% final) for analysis via western blot. Fractionation efficiency was confirmed by western blot using an antibody against they synaptically localized protein synaptophysin (SY38 0.3µg/mL, Chemicon). Synaptophysin was enriched throughout the fractionation process indicating successful enrichment of synaptic proteins.

2.7. Hippocampal cultures

Low density hippocampal cultures were prepared from newborn (P0) mice. Briefly, pups were decapitated and dissected hippocampi were placed in Hank's balanced salt solution (Gibco) supplemented with sodium bicarbonate (4mM), HEPES (10mM) and a mix of penicillin and streptomycin (Gibco). Subsequently, hippocampi were dissociated: first enzymatically using trypsin (0.25% trypsin 15 min 37˚C), and then mechanically by gentle trituration with fire-polished Pasteur pipettes of decreasing diameters. Neurons were plated at a density of ~ 12,000 cells/cm^2 onto glass coverslips pre-coated with poly-L-lysine (1mg/mL) and bathed in a plating medium consisting of MEM (Gibco) supplemented with horse serum (10%; Gibco), glucose (0.6%), Glutamax (2mM; Gibco), and sodium pyruvate (1mM). After allowing the cells to adhere for 3 hours, the medium was replaced with growing media consisting of Neurobasal A (Gibco) media supplemented with B27 (Gibco). Arabinofuranosylcytosine (Ara-C; 5 μM) was added 6 days after plating to limit proliferation of non-neuronal cells. For mixed genotype cultures, ~6,000 cells/cm^2 of each genotype were plated together per coverslip. Cells were then processed for immunostaining at 16-20DIV.

For β_2m treated cultures, 16DIV hippocampal cultures were treated with 10μM of recombinant β_2m (Sigma M4890) for 1 hour in conditioned media. Cells were the fixed and immunostained as described.

2.8. Live labeling of cultured hippocampal neurons

Hippocampal neurons (16 DIV) were live labeled 15 min at 37˚C in the presence of 50μM FITC-conjugated insulin (Molecular Probes) diluted in conditioned media.

After 2 washes in ice cold PBS, neurons were fixed 20 min at RT in a solution of 4% PFA/4% sucrose in PBS. Excess PFA was quenched 10 min at RT in PBS/ 100mM glycine followed by 4 brief washes in blocking buffer and one final wash in PBS. Cells were then visualized using standard fluorescent microscopy.

2.9. Electron microscopy

Mice were perfused with 1X PBS at 37°C, followed by 2% PFA/2.5% Glutaraldehyde in 0.1M sodium cacodylate (pH 7.4). Brains were dissected out and post-fixed O/N at 4°C, and thick sectioned on a vibratome (300μm; coronal). The 7 thick sections containing the anterior hippocampus were obtained for each animal and the 2nd section was chosen for consistency between animals and processed. Following 3 washes in sodium cacodylate for 15 min and 2 washes in ddH2O, sections were incubated in 1% OsO4/0.5% potassium ferrocyanate for 1 hour, washed in ddH2O, incubated in 1% uranyl acetate 30 min, washed in ddH2O, dehydrated in an EtOH series, incubated in SciPoxy resin/EtOH without DMP30 for 48hours at 65°C, incubated in pure resin without DMP30 under vacuum for 1 hour, incubated with DMP30 1 hour, cut into thin ~90nm (silver) sections and mounted on Formvar/carbon slot grids. EM images were collected at 10,000x magnification. For CA3, images were collected in stratum lucidum, at the center of the curve of CA3, exactly 50μm from the pyramidale cell layer. For CA1, images were collected in stratum radiatum, directly above the upper tip of the dentate and 50μm from the CA1 pyramidal cell layer. Care was taken to image non-overlapping areas. Synapses were counted blind to genotype in 15 images from CA3 and 15 from

CA1 for each animal (n=6 WT mice, n=6 $\beta 2m^{-/-}TAP^{-/-}$ and n=3 $K^{b-/-}D^{b-/-}$), representing a total area of 390μm^2 per animal in CA3 or CA1.

2.10. Blood glucose concentrations

Fasting blood glucose concentrations were taken from 6-month-old male or female mice using blood from a tail puncture samples. Blood glucose levels were then measured using a Precision Xtra blood glucose monitor (MediSense). All blood glucose measurements were taken between 8-10am after exactly 24 hours of fasting (n=12 WT male mice, n=19 $\beta 2m^{-/-}TAP^{-/-}$ male mice, n=8 WT female mice and n=19 $\beta 2m^{-/-}TAP^{-/-}$ female mice).

2.11. Food intake and body weight studies

To measure food intake 4-month-old male or female mice were placed in a cage with a pre-weighed amount of food. Food was then weighed every day for four days and the average amount of food consumed per day was determined. Mouse body weight was also measured each day for four days and the average weight determined for each animal. Food intake, measured in food consumed per day per mouse in milligrams, was normalized to mouse body weight, measured as average body weight of a mouse over a 4 day period in grams (n=15 WT male mice, n=15 $\beta 2m^{-/-}TAP^{-/-}$ male mice, n=19 WT female mice and n=14 $\beta 2m^{-/-}TAP^{-/-}$ female mice).

2.12. Statistics

For all experiments, means are reported ± standard error of the mean (SEM). Statistical comparisons of the data were performed using GraphPad InStat v.3.06 for Windows (GraphPad Software).

3 RESULTS

3.1. IR proteins are expressed in neurons

Previous studies using radiolabeled insulin suggest that IR are extensively expressed in mammalian brain (Havrankova et al., 1978; Kar et al., 1997; Unger et al., 1989). However, this labeling includes insulin binding to other receptors, including IGF-1 receptors. To specifically characterize the expression of IR in the brain, we performed immunostaining on P30 mouse brains using an antibody against an intracellular region of the β-subunit of IR (clone C19). This antibody is specific for IR and does not cross-react with IGF receptors (Baudler et al., 2005; Entingh-Pearsall and Kahn, 2004). IR were detected in many brain regions, including the cortex, where it labeled deep and superficial layers, the cerebellum, where it labeled processes ensheathing cerebellar Purkinje cells, and the hippocampus, where it labeled fibers in stratum lucidum in the CA3 region. Notably, hippocampal staining for IR was intense in CA3 but completely absent in CA1 (Figure 3.1.1.).

To determine if neuronal IR are expressed in axons or dendrites, we co-immunostained hippocampal slices for IR and markers for dendrites (MAP2) or axons (TAU). IR co-localized with the axonal marker TAU, but not the dendritic marker MAP2, in CA3 (Figure 3.1.2.). The axons that express IR in this region likely represent dentate granule cell axons (mossy fibers), based on their location and orientation. This was confirmed by co-localization of IR with staining for the dentate granule cell marker calbindin in hippocampal sections and in hippocampal neurons in culture (Figure 3.1.3.). In the cerebellum, the processes ensheathing the Purkinje cells that express IR likely represent basket cell axons based on their location and unique morphology. IR

expression in basket cell axons was confirmed by co-localization of IR with Parvalbumin, a marker for basket cells (Figure 3.1.4.).

3.2. MHCI and IR are expressed in close apposition in brain

To determine if MHCI and IR are co-expressed in neurons, we next performed double-label immunohistochemistry with antibodies against MHCI and IR. Previous studies show that MHCI is primarily expressed in the somatodendritic compartment of cerebellar and hippocampal neurons (Goddard et al., 2007; Letellier et al., 2008; McConnell et al., 2009). Consistent with this, we observed MHCI immunoreactivity in the soma and dendrites of cerebellar Purkinje cells and hippocampal pyramidal cells. IR were closely apposed to MHCI-positive puncta in both cerebellum and hippocampus (Figure 3.2.1.). This included strong MHCI immunoreactivity in CA3 pyramidal cells, which are the postsynaptic targets for IR-positive mossy fiber axons. Thus IR and MHCI are expressed in apposing pre- and post-synaptic cells respectively, indicating these proteins could interact from across the cell, i.e., in *trans*.

3.3. IR proteins associate with MHCI in hippocampal lysates

To determine if MHCI can form a complex with neuronal IR, western blotting and co-immunoprecipitation experiments were performed. Western blots of WT hippocampal lysates revealed two specific MHCI-immunoreactive bands, a stronger 45kDa band and a weaker 55 kDa band, as previously reported (Huh et al., 2000). IR and associated proteins were precipitated from WT hippocampal lysates using IRβ antibodies. Immunoprecipitation of IR from hippocampus co-precipitated the 55kDa MHCI band,

but not the abundant intracellular protein GAPDH or the synaptic cell surface protein GluR1, indicating MHCI can interact, either directly or indirectly, with IR. Immunoprecipitation with an IgG isotype control antibody did not pull down detectable IR or MHCI proteins (Figure 3.3.1.). Together, these data demonstrate that MHCI and IR are expressed in close apposition in many brain regions and form a complex in hippocampal lysates.

3.4. IR immunostaining is abolished in *β2m$^{-/-}$TAP$^{-/-}$* neurons

Since MHCI can interact with neuronal IR, we reasoned that changes in MHCI levels of expression might affect the expression or function of IR in the brain. To test this, we compared expression of IR in brains from WT and MHCI-deficient *β2m$^{-/-}$TAP$^{-/-}$* mice (see methods). As shown above, extensive labeling of IR with the IRβ (C19) antibody is present in WT hippocampus. Strikingly, immunostaining for IR with the same antibody was completely abolished in *β2m$^{-/-}$TAP$^{-/-}$* hippocampal slices (Figure 3.4.1.). This finding was also seen with the IRβ (RTK) antibody in hippocampal slices (Figure 3.4.2.). Similarly, strong immunolabeling of IR was detected in a subset of WT hippocampal neurons in culture (presumable dentate granule cells), but labeling was not detectable in *β2m$^{-/-}$TAP$^{-/-}$* hippocampal neurons (Figure 3.4.3.).

The loss of immunostaining of IR in *β2m$^{-/-}$TAP$^{-/-}$* hippocampal neurons could be due to unknown effects of β2m or TAP rather than their effects on MHCI expression. However immunolabeling experiments using *K$^{b-/-}$D$^{b-/-}$* mice, which lack the classical MHCI genes H2D and H2K but have normal levels of β2m and TAP (Vugmeyster et al., 1998), revealed a significant dampening of immunolabeling of IR (Figure 3.4.4.). A

reduction, rather than a loss, of immunostaining or IR in $K^{b-/-}D^{b-/-}$ mice, who lack only two of the many MHCI genes, argues that functional redundancy among MHCI family members may exist and that more than one type of MHCI molecule can interact with IR. Taken together, these data indicate that MHCI proteins are required for normal immunodetection of IR in hippocampal neurons using the C19 and RTK antibodies.

3.5. Total, surface and synaptic levels of IR protein, and mossy fiber immunolabeling are normal in *β2m*$^{-/-}$*TAP*$^{-/-}$ hippocampus

Why is immunostaining for IR abolished in the brains of *β2m*$^{-/-}$*TAP*$^{-/-}$ mice? One possibility is that *β2m*$^{-/-}$*TAP*$^{-/-}$ neurons express lower protein levels of IR. To test this, we performed western blots on hippocampal lysates. Unexpectedly, despite the complete inability to immunolabel native IRβ using the C19 antibody in *β2m*$^{-/-}$*TAP*$^{-/-}$ hippocampus, denatured IRβ protein was readily detectable in western blots of *β2m*$^{-/-}$*TAP*$^{-/-}$ hippocampal lysates using the same antibody. Densiometric quantification of the IR bands revealed that total levels of IR protein were indistinguishable from WT in *β2m*$^{-/-}$*TAP*$^{-/-}$ hippocampal lysates (Figure 3.5.1.). Similar results were obtained from western blots of whole brain lysates and from blots using two additional IR antibodies (RTK and N20; controls not shown).

Another possibility to explain the selective loss of IR immunostaining in *β2m*$^{-/-}$ *TAP*$^{-/-}$ mice is due to a change in the subcellular localization of the IR protein. For example, IR could be sequestered in an intracellular compartment that renders it inaccessible to antibodies in intact tissue slices, but does not affect detection in brain homogenates via western blotting. To examine cellular distribution of IR, we performed

two sets of experiments. First, to label cell surface IR, we performed surface biotinylation experiments on live hippocampal slices. Surface levels of IR were comparable in WT and *β2m*$^{-/-}$*TAP*$^{-/-}$ hippocampus (Figure 3.5.1.). We did not detect the abundant intracellular protein GAPDH, confirming this technique selectively labeled cell surface proteins. Next, we performed subcellular fractionation experiments on hippocampal lysates from WT and *β2m*$^{-/-}$*TAP*$^{-/-}$ mice. Synaptic levels of IR were indistinguishable between the two genotypes (Figure 3.5.2.). Thus the loss of IRβ (C19) immunostaining cannot be explained by a change in total, cell surface or synaptic levels of IR in *β2m*$^{-/-}$*TAP*$^{-/-}$ neurons.

A third possibility to explain the loss of IR immunostaining in *β2m*$^{-/-}$*TAP*$^{-/-}$ neurons is that these mice have a loss of IR expressing axons. However, calbindin labeling of dentate granule cells, which express IR in their mossy fiber axons, was grossly normal in *β2m*$^{-/-}$*TAP*$^{-/-}$ hippocampus (Figure 3.5.3.). Calbindin labeling was also normal in dissociated *β2m*$^{-/-}$*TAP*$^{-/-}$ hippocampal cultures, both in number of calbindin-expressing cells and in calbindin expression patterns (data not shown). Thus, the loss of IR immunostaining in *β2m*$^{-/-}$*TAP*$^{-/-}$ hippocampus cannot be explained by altered cellular distribution or a loss of IR-positive mossy fiber axons.

3.6. IR is detected by immunostaining in *β2m*$^{-/-}$*TAP*$^{-/-}$ neurons using reagents against alternative IR epitopes or following epitope unmasking

The paradoxical, genotype-specific loss of IRβ immunostaining in *β2m*$^{-/-}$*TAP*$^{-/-}$ neurons despite the presence of normal levels of IR protein could reflect changes in the epitope where the IRβ (C19) antibody binds. Changes in conformation or protein-protein

interactions at this epitope could prevent antibody binding to the native protein but would not be expected to affect antibody binding under the denaturing conditions of western blotting. In addition, such changes might not affect binding to other domains. To explore this, three separate experiments were performed.

First, to test insulin binding to native cell surface receptors in WT and *β2m*$^{-/-}$*TAP*$^{-/-}$ hippocampal neurons we live-labeled cultured neurons with fluorescein-conjugated recombinant insulin (FITC-insulin). Insulin binds to an extracellular domain of the IR α-subunit. Brief application of FITC-insulin to WT neurons yielded punctate labeling of the neurites and soma (Figure 3.6.1.). This labeling, which represents insulin binding to IR as well as some IGF-1R, was qualitatively indistinguishable from WT in *β2m*$^{-/-}$*TAP*$^{-/-}$ neurons. This is consistent with surface biotinylation experiments above which show that cell surface levels of IR are normal in *β2m*$^{-/-}$*TAP*$^{-/-}$. Furthermore, it reveals that *β2m*$^{-/-}$ *TAP*$^{-/-}$ neurons are competent to bind insulin at the extracellular ligand binding domain.

Next, to further examine antibody binding to native IR we used antibodies raised against other epitopes of IR to immunostain WT and *β2m*$^{-/-}$*TAP*$^{-/-}$ hippocampal neurons. As above, immunostaining with the IRβ (C19) antibody was completely abolished in *β2m*$^{-/-}$*TAP*$^{-/-}$ neurons (Figure 3.6.1.). In contrast, immunostaining with two additional IR antibodies showed robust IR labeling in *β2m*$^{-/-}$*TAP*$^{-/-}$ neurons. Of note, these antibodies do not share an epitope with C19, but rather were raised against an extracellular region of the IR β-subunit (clone D17) or an extracellular portion of the IR α-subunit (clone N20). All antibody labeling resulted in strong immunostaining in both WT and *β2m*$^{-/-}$*TAP*$^{-/-}$ hippocampal neurons.

Finally, to determine if IRβ (C19) immunolabeling is abolished in *β2m*$^{-/-}$*TAP*$^{-/-}$ neurons due to masking of the relevant epitope, unmasking experiments were performed. Antigen or epitope unmasking is a technique in which thermal or chemical conditions are used to partially denture proteins *in situ* (Shi et al., 2001). While IRβ (C19) antibodies failed to detect IR protein in *β2m*$^{-/-}$*TAP*$^{-/-}$ neurons, IR staining with this same antibody was unmasked in *β2m*$^{-/-}$*TAP*$^{-/-}$ neurons following antigen retrieval (Figure 3.6.2.). Of note, application of exogenous insulin or the exogenous MHCI light chain, β2m, were not sufficient to rescue the loss of IR immunolabeling in *β2m*$^{-/-}$*TAP*$^{-/-}$ animals (Figures 3.6.3. and 3.6.4.). Thus, three separate lines of evidence suggest that an intracellular epitope of the IR β-subunit is modified in *β2m*$^{-/-}$*TAP*$^{-/-}$ neurons, likely through MHCI-dependent epitope masking.

3.7. IRβ immunostaining is restored in *β2m*$^{-/-}$*TAP*$^{-/-}$ neurons co-cultured with WT neurons

Our data shows that MHCI and IR can associate in hippocampal lysates and their expression pattern in *vivo* suggests that pre-synaptic IR may interact with post-synaptic MHCI (i.e. in *trans*). Furthermore, we have shown that lack of surface expression of MHCI in *β2m*$^{-/-}$*TAP*$^{-/-}$ neurons leads to an inability of the IRβ (C19) antibody to detect IR because the c-terminal epitope recognized by this antibody is masked in the absence of MHCI (Figure 3.7.1. and 3.7.2.). We reasoned then that if MHCI and IR proteins interact in *trans*, co-culturing *β2m*$^{-/-}$*TAP*$^{-/-}$ neurons with WT, MHCI-expressing neurons might rescue the loss of IRβ (C19) immunolabeling in *β2m*$^{-/-}$*TAP*$^{-/-}$ neurons. To test this, we co-cultured WT neurons (identified by expression of actin-GFP; see Methods) and *β2m*$^{-/-}$

TAP$^{-/-}$ hippocampal neurons, and assayed for rescue of IRβ (C19) immunostaining in *β2m*$^{-/-}$*TAP*$^{-/-}$ (GFP-negative) neurons. One hundred percent of the cells in pure WT actin-GFP cultures expressed GFP, and at the density plated, on average seventeen cells per coverslip were IRβ (C19)-positive (Figure 3.7.3), presumably representing the dentate granule cells that express IR in hippocampal slice. On the contrary, none of the cells in pure *β2m*$^{-/-}$*TAP*$^{-/-}$ cultures expressed GFP or showed labeling for IRβ with the C19 antibody as expected. When neurons of the two genotypes were cultured together in the same dish in equal quantities, however, two distinct C19-positive populations were seen: (1) GFP-positive neurons, which represent WT cells expressing detectable IRβ, and (2) a small number of GFP-negative neurons, which represent *β2m*$^{-/-}$*TAP*$^{-/-}$ cells on which IRβ (C19) labeling has been rescued (Figure 3.7.3). Since all WT neurons unambiguously express GFP, and *β2m*$^{-/-}$*TAP*$^{-/-}$ neurons never show detectable IRβ (C19) staining, the presence IRβ (C19) immunostaining in GFP-negative cells conclusively demonstrates that the disruption of the C19 epitope in *β2m*$^{-/-}$*TAP*$^{-/-}$ neurons can be rescued by the presence of WT neurons. This rescue is consistent with a *trans* interaction between MHCI on WT neurons and IR on *β2m*$^{-/-}$*TAP*$^{-/-}$ neurons.

3.8. IR is constitutively phosphorylated in *β2m*$^{-/-}$*TAP*$^{-/-}$ neurons

IR activation involves autophosphorylation of IR on tyrosine residues and subsequent recruitment and activation of downstream second messengers that mediate IR signaling (Hubbard et al., 1994). To determine whether MHCI increases IR activation, we examined tyrosine phosphorylation of the IR in WT and *β2m*$^{-/-}$*TAP*$^{-/-}$ animals. Live

hippocampal slices were incubated in phosphatase inhibitors in the presence or absence of insulin, and the immunoprecipitated IRs were probed with antibodies against phosphotyrosine in western blots. As expected, IR from WT slices was not detectably phosphorylated on tyrosine residues, but became rapidly phosphorylated upon exposure to exogenous insulin (Figure 3.8.1.). In contrast, IR precipitated from *β2m*$^{-/-}$*TAP*$^{-/-}$ hippocampus showed significant basal phosphorylation of IR, even in the absence of insulin treatment. This tonic phosphorylation of IR in the absence of MHCI was similar in magnitude to insulin-stimulated IR phosphorylation in WT mice. Furthermore, application of insulin did not increase IR phosphorylation in *β2m*$^{-/-}$*TAP*$^{-/-}$slices, reflecting either the occlusion or failure of insulin-induced IR phosphorylation in *β2m*$^{-/-}$*TAP*$^{-/-}$slices. Preliminary experiments reveal that PI3K, a downstream signaling molecule that is phosphorylated by IR, is also activated under basal conditions in *β2m*$^{-/-}$*TAP*$^{-/-}$ mice (Figure 3.8.2.). Thus, in the absence of cell surface MHCI, IR is constitutively activated.

3.9. Synapse number is increased in hippocampal CA3, but not CA1, of *β2m*$^{-/-}$*TAP*$^{-/-}$ mice

A recent study of neuronal IR function in *Xenopus* reveals that IR regulates synapse number in developing tectum. Specifically, reduction of IR signaling using a dominant negative form of IR is associated with a decrease in synapse density in *Xenopus* tectum (Chiu et al., 2008). Therefore, we hypothesized that if MHCI regulates IR activity, synapse density might be altered in MHCI-deficient *β2m*$^{-/-}$*TAP*$^{-/-}$hippocampus. Furthermore, we predicted that the change in synapse number would be restricted to regions where IR is normally expressed. To test this, we performed electron microscopy

and counted synapses in stratum lucidum of CA3 and stratum radiatum of CA1 in P30 mice. Stratum lucidum contains synapses between IR-expressing mossy fiber axons and MHCI-expressing CA3 pyramidal cells, while stratum radiatum of CA1 contains synapses made by neurons that express MHCI but do not express IR. Synapses were defined as areas where post-synaptic densities were closely apposed to pre-synaptic boutons, identified by the presence of synaptic vesicles, and the number of synapses per 400μm^2 of neuropil was used to calculate synapse density. Synaptic ultrastructure was qualitatively similar in WT and knockout animals in both CA3 and CA1 (Figure 3.9.1.). We found that MHCI-deficient *β2m$^{-/-}$TAP$^{-/-}$* mice had more synapses per area than WT mice in area CA3, where IR is expressed, but not area CA1, where IR is not expressed (Figure 3.9.1.). Similar results were seen in *K$^{b-/-}$D$^{b-/-}$* mice, which specifically lack the classical MHCI genes H2-K and H2-D, but do not have mutations in the β2m or TAP genes (Vugmeyster et al., 1998). Thus, MHCI limits synapse density in areas of IR expression, but not in areas where IR is not expressed. Furthermore, since reduction of IR signaling caused a reduction in synapse number in other systems, the increase in synapse number in CA3 raises the possibility that IR signaling is enhanced in MHCI-deficient brain.

3.10. Fasted blood glucose levels are normal in *β2m$^{-/-}$TAP$^{-/-}$* mice

Outside the brain, IR signaling is known to regulate blood glucose levels. To test whether blood glucose concentrations are altered in *β2m$^{-/-}$TAP$^{-/-}$* mice we performed analysis on blood samples from tail punctures in fasted WT and *β2m$^{-/-}$TAP$^{-/-}$* mice. After 24-hours of fasting, *β2m$^{-/-}$TAP$^{-/-}$* mice had comparable blood glucose levels to WT

animals (Figure 3.10.1.). Thus, MHCI-deficient animals do not have a change in their fasted blood glucose levels suggesting that changes seen in IR signaling in the hippocampus of MHCI-deficient mice do not affect peripheral glucose metabolism in these animals.

3.11. Food intake is normal but body weight is decreased in *β2m*$^{-/-}$*TAP*$^{-/-}$ mice

IR signaling in neurons has been shown to play a role in neuronal control of body weight and food intake. Neuron-specific insulin receptor knockout (NIRKO) mice display gender-specific changes in a body weight and food intake revealing a role for neuronal IR in these processes. Specifically, female NIRKO mice display an increase in body weight as compared to controls from 6 to 23 weeks of age. On the other hand, male NIRKO mice do not show an increase in body weight until after 24 weeks of age. Regarding food intake in these animals, female NIRKO mice consume more food than WT controls as measured by milligrams of food consumed per gram of body weight per mouse (on a regular chow diet), while male NIRKO mice do not show differences in the amount of food they consume versus controls (Bruning et al., 2000).

Given that *β2m*$^{-/-}$*TAP*$^{-/-}$ mice have altered neuronal IR signaling, we wanted to test for changes in body weight and food intake in these animals. To do this we performed the following experiments. First, cohorts of WT and *β2m*$^{-/-}$*TAP*$^{-/-}$ mice of both genders were weighed at 6, 10, 14, 18, 22, 26 and 70 weeks. *β2m*$^{-/-}$*TAP*$^{-/-}$ male mice weighed significantly less that WT male mice at all ages measured, while female *β2m*$^{-/-}$*TAP*$^{-/-}$ mice did not show a change in body weight until after 24 weeks of age (Figure 3.11.1.). Of note, this is the same finding seen in NIRKO mice, but in the opposite gender.

Next, we measured food consumption in 20 week old male and female animals over a four day period. *β2m*$^{-/-}$*TAP*$^{-/-}$ animals did not display any significant changes in the amount of food they consumed as compared to WT. However, when food intake was normalized to body weight, *β2m*$^{-/-}$*TAP*$^{-/-}$ mice consumed significantly more food per gram of body weight that WT animals (Figure 3.11.2.). This is the same result seen previously in NIRKO mice but is again in the opposite gender.

The opposing gender-specific phenotypes seen between *β2m*$^{-/-}$*TAP*$^{-/-}$ and NIRKO mice complicate the interpretation of these experiments and several possible explanations for these observations exist. One possibility is that IR, MHCI or both have differential effects in the body when exposed to male versus female hormones. Indeed evidence supports this idea given that IR knockout mice have differential systemic readouts in male versus female mice (Bruning et al., 2000; Fisher et al., 2005). A second possibility is that strain differences between the *β2m*$^{-/-}$*TAP*$^{-/-}$ (C57BL/6) and NIRKO (BALB/c) mouse lines prevent phenotypic comparison between the two species/genders. It is known that genetic knockout of the MHCI-like gene *HFE* (a gene that when knocked out causes iron accumulation disease) in different mouse strains can lead to significant variability in the severity of the disease. Not only do certain strains of *HFE* knockout mice display increased disease progression, but female HFE knockout mice had increased iron accumulation beyond their strain-matched male counterparts (Fleming et al., 2001; Sproule et al., 2001). It is therefore possible that strain differences account for the differences we see in feeding behavior of *β2m*$^{-/-}$*TAP*$^{-/-}$ and NIRKO mice.

3.12. Summary of IR signaling in WT and *β2m*$^{-/-}$*TAP*$^{-/-}$ mice

The data present here demonstrate, for the first time, that MHCI interacts with IR in neurons. Endogenous MHCI acts as a negative regulator of neuronal IR signaling and synapse number in the hippocampus (Figure 3.12.1.). This regulation likely involves an allosteric modification of an intracellular epitope of the IR by endogenous MHCI and suggests that a broader role of MHCI in neurons may be to act as a negative regulator of cell surface receptors.

Chapters 3 and 4, in part, have been submitted for publication of the material as it may appear in Neuron, 2009, Dixon-Salazar, Tracy; Fourgeaud, Lawrence; Boulanger, Lisa, Cell Press, 2009. The dissertation author was the primary investigator and author of this paper.

4 DISCUSSION

Growing evidence suggests that MHCI plays unexpected, non-immune roles in the developing and adult brain. Here we show that MHCI is a novel regulator of IR signaling and synapse number in neurons. MHCI and IR proteins associate in neurons, and genetic reduction of cell surface levels of MHCI modifies IR signaling. Together, immunostaining, biochemistry and labeled-ligand studies suggest that an epitope in the c-terminus of the IR β-subunit is masked in MHCI-deficient *β2m*$^{-/-}$*TAP*$^{-/-}$ animals. The site of this apparent masking includes two key tyrosine residues that are autophosphorylated upon insulin binding and required for subsequent downstream IR signaling (Hubbard et al., 1994; Lamothe et al., 1995; Van Horn et al., 1994; White and Kahn, 1994). Masking of this epitope in *β2m*$^{-/-}$*TAP*$^{-/-}$ animals is associated with an increase in basal tyrosine phosphorylation of IR that occludes further insulin-induced phosphorylation. This increase in IR signaling is associated with an increase in synapse density, a process known to be regulated by IR signaling, specifically in regions of the hippocampus where IR is expressed. Collectively, our results suggest that endogenous MHCI acts as a negative regulator of IR signaling and synapse number in neurons.

Characterization of IR expression in brain

This study represents the most comprehensive characterization of IR protein expression in rodent brain to date. IR is expressed widely in mouse brain (Figure 3.1.1.), with robust labeling in cortex, hippocampus and cerebellum. IRβ co-localized with axonal (TAU) and dentate granule cell (calbindin) markers in the hippocampus

suggesting IR is expressed in mossy fiber axons in the hippocampus (Figures 3.1.2. and 3.1.3.). These findings are consistent with previous studies using radiolabeled insulin to show ligand binding in these brain regions (Kar et al., 1993). Other studies, however, have shown that IR expression in the hippocampus is found in pyramidal cells (Abbott et al., 1999; Zhao et al., 1999). The IRβ (C19) antibody used here did not detect IR in pyramidal cell bodies in hippocampal sections; however C19, as well as other IR antibodies, did detect IR in pyramidal cell somas in dissociated hippocampal cultures (Figure 3.4.3. and 3.6.1.). These differences in staining could be due to intrinsic differences in protein expression of IR in sections versus cultures; however other likely explanations include the IRβ (C19) antibody labels only a subset of IR found in brain, or antibodies used in previous studies may recognize both IR and the similar IGF-1R. Further studies are needed to further tease apart the full extent of IR and IGF-1R protein expression in brain.

MHCI and IR interact in neurons

Previous studies in non-neuronal cell types suggest MHCI and IR may interact. The interaction between MHCI and IR in neurons, however, has never been characterized. Our data provide the first evidence that MHCI and IR can interact in the mammalian brain. Both MHCI and IR are expressed in close proximity in cerebellum and hippocampus and can form a complex in hippocampal lysates. Consistent with the idea that MHCI interacts with neuronal IR, immunostaining for IRβ was completely abolished in MHCI-deficient hippocampus. It is possible that the loss of IRβ staining in *β2m*$^{-/-}$*TAP*$^{-/-}$ mice is due to novel functions of β2m or TAP proteins in regulating IR

structure or function. Two lines of evidence, however, argue against this. First, MHCI proteins co-immunoprecipitated with IR in hippocampal homogenates (Figure 3.3.1.). Next, immunolabeling for IR in $K^{b-/-}D^{b-/-}$, which lack the classical MHCI molecules H2K and H2D but have normal levels of β2m and TAP, showed a decrease in IR detectability as compared to WT (Figure 3.4.4.). Taken together these data support the conclusion that it is MHCI, not β2m or TAP, that interacts with neuronal IR and regulates its function.

Evidence for a *trans* interaction between MHCI and IR in neurons

MHCI binds to several immunoreceptors, most notably the T-cell receptor, on neighboring cells (i.e. in *trans*). In a similar fashion, two of our current results suggest that MHCI and IR interact in *trans* in neurons. First, in CA3 of hippocampus, axonal (pre-synaptic) expression of IR proteins but somatodendritic (post-synaptic) expression of MHCI suggests that MHCI and IR could interact across the mossy fiber-CA3 synapse (Figure 3.2.1.). Second, IRβ (C19) immunolabeling could be rescued in $\beta 2m^{-/-}TAP^{-/-}$ hippocampal neurons when cultured with WT neurons (Figure 3.7.1., 3.7.2, 3.7.3.). One possible explanation for this rescue is that WT cells release soluble β2m thereby allowing $\beta 2m^{-/-}TAP^{-/-}$ neurons to regain normal expression of their IR. However, application of purified β2m to $\beta 2m^{-/-}TAP^{-/-}$ neurons did not restore IRβ (C19) immunolabeling in these cells (Figure 3.6.4.). Thus, it is possible that a direct interaction between WT and $\beta 2m^{-/-}TAP^{-/-}$ neurons restores the IR immunostaining in $\beta 2m^{-/-}TAP^{-/-}$ cells. It is also possible that MHCI affects the secretion of other soluble factors (i.e. insulin) and this, in turn, affects IR labeling and phosphorylation. The apposition of MHCI and IR and the rescue of labeling provide the first evidence that MHCI and IR may interact in neurons in *trans.*

IR c-terminal modification by MHCI

There is a selective loss of IR immunostaining in *β2m*$^{-/-}$*TAP*$^{-/-}$ animals using an antibody against a c-terminal epitope of IRβ. This loss of IR immunostaining is not due to changes in the protein levels or localization of IR protein, as these are normal in *β2m*$^{-/-}$ *TAP*$^{-/-}$ animals (Figures 3.5.1. and 3.5.2.). Similarly, it is not due to a technical limitation of the antibody, since the loss of IR labeling is genotype-specific and C19 gives robust labeling of IR in WT neurons (Figures 3.4.1. and 3.4.3.). Instead, it is likely that an epitope of IR is masked in the absence of MHCI. Indeed, immunostaining using two IR antibodies directed against distinct epitopes of IR produced labeling of IR in *β2m*$^{-/-}$*TAP*$^{-/-}$ neurons (Figure 3.6.1.). In addition, the IRβ (C19) antibody failed to detect native IR in immunostaining of *β2m*$^{-/-}$*TAP*$^{-/-}$ neurons, but was effective in detecting denatured IR in western blotting of *β2m*$^{-/-}$*TAP*$^{-/-}$ neuronal lysates (Figures 3.5.1.), and IR immunolabeling with IRβ (C19) antibody was unmasked in *β2m*$^{-/-}$*TAP*$^{-/-}$ neurons following antigen retrieval (Figure 3.6.2.). Thus, several distinct sets of experiments suggest that endogenous MHCI modifies an intracellular epitope of the IR β-subunit. If MHCI and IR interact in *trans*, this may happen through allosteric mechanisms.

Functional consequences of IR modification by MHCI

The epitope masked in MHCI-deficient neurons contains two tyrosine residues that are phosphorylated upon insulin binding and a PI3K binding motif leading us to postulate that a change in this epitope may lead to a change in IR signaling. Indeed, IR is constitutively phosphorylated on tyrosine residues in *β2m*$^{-/-}$*TAP*$^{-/-}$ animals (Figure 3.8.1.), leading to an increase in basal IR signaling (Hubbard et al., 1994).

What is the consequence of constitutive IR signaling in *β2m*$^{-/-}$*TAP*$^{-/-}$ neurons? IR signaling has been extensively studied in peripheral tissues as a regulator of blood glucose levels but the role of neuronal IR is less well-defined. Rather than regulating glucose uptake, neuronal insulin and IR have been implicated in specific events in brain development and function. A recent study using acute transfection of *Xenopus* tectal neurons with constructs encoding WT or dominant negative IR shows neuronal IR signaling is a positive regulator of synapse density (Chiu et al., 2008). Likewise, our results show that *β2m*$^{-/-}$*TAP*$^{-/-}$ mice which have increase IR signaling also have an increase in synapse number specifically in areas of IR expression in hippocampus (Figure 3.9.1.*)*. Our current results raise the possibility that this increase in synapse number may be directly regulated by the increase in IR signaling seen in *β2m*$^{-/-}$*TAP*$^{-/-}$ animals.

In closing, the data present here demonstrate, for the first time, that MHCI interacts with IR in neurons. Endogenous MHCI acts as a negative regulator of neuronal IR signaling and synapse number in the hippocampus (Figure 3.12.1.). This regulation likely involves an allosteric modification of an intracellular epitope of the IR by endogenous MHCI and suggests that a broader role of MHCI in neurons may be to act as a negative regulator of cell surface receptors.

Chapters 3 and 4, in part, have been submitted for publication of the material as it may appear in Neuron, 2009, Dixon-Salazar, Tracy; Fourgeaud, Lawrence; Boulanger, Lisa, Cell Press, 2009. The dissertation author was the primary investigator and author of this paper.

APPENDIX

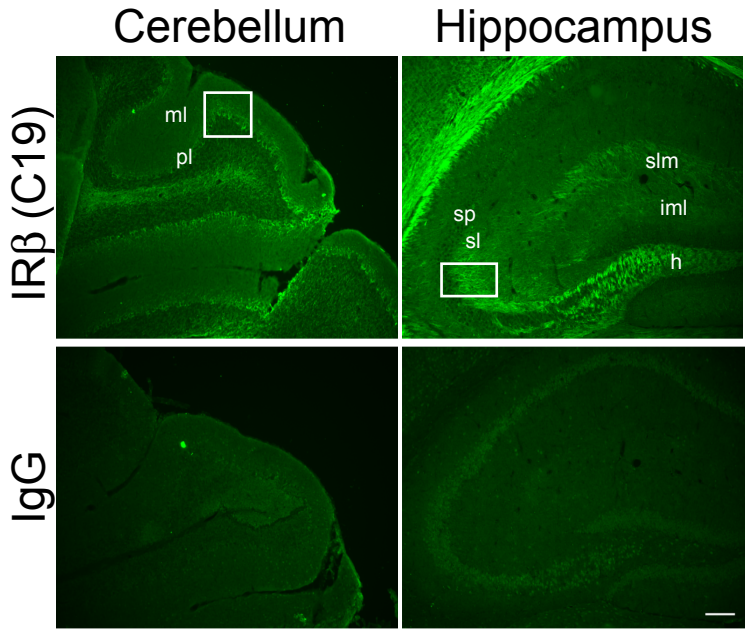

Figure 3.1.1. Insulin receptor (IR) proteins are expressed in the brain. Coronal sections of P30 mouse brain immunostained with IRβ (C19) antibodies or IgG isotype control. Strong, specific IR staining is observed in fibers surrounding cerebellar Purkinje cells, and in stratum lucidum (sl), hilus (h), stratum layer moleculare (slm), and inner molecular layer (iml), but not stratum pyramidale (sp), of hippocampus. Boxed regions are magnified in Figures 3.1.2, 3.1.4, 3.2.1, 3.4.1, 3.4.2, 3.6.2 and 3.6.3. Scale 100μm.

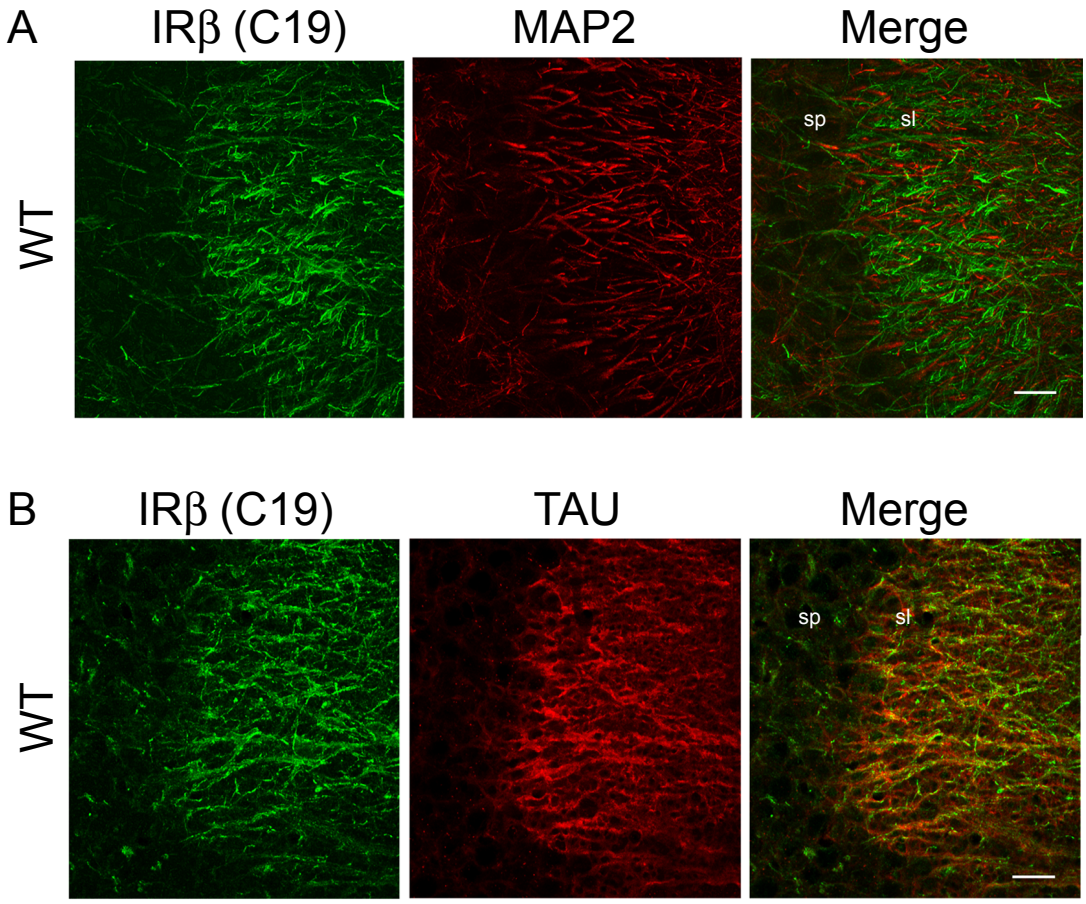

Figure 3.1.2. IR co-localizes with axonal but not dendritic markers in hippocampal neurons. (A) Double-label immunohistochemistry for IRβ (*green*) and the dendritic marker MAP2 *(red)*. IR does not co-localize with MAP2 in stratum lucidum (sl) of WT hippocampus (*merge*). Scale 20µm. (B) Double-label immunohistochemistry for IRβ (*green*) and the axonal marker TAU *(red)*. IR co-localizes with TAU in stratum lucidum (sl) of WT hippocampus (*merge*). Scale 20µm.

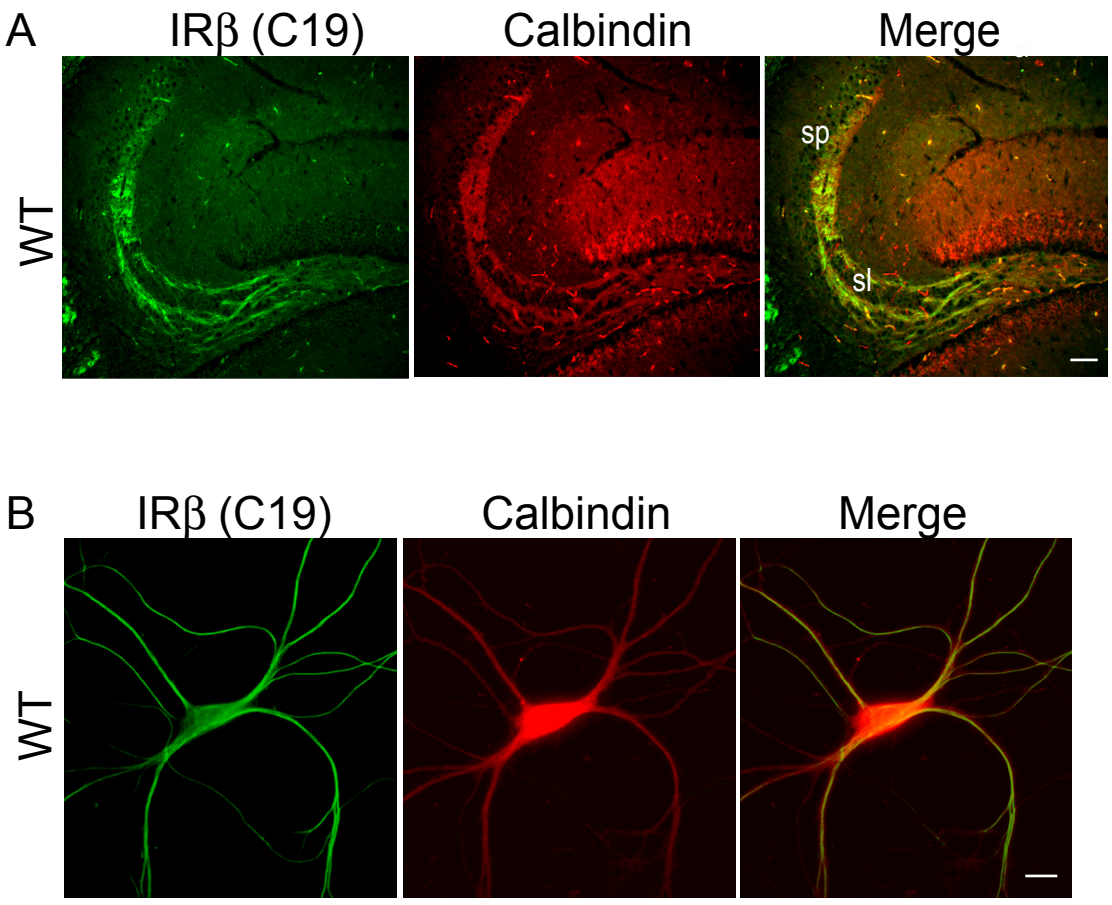

Figure 3.1.3. IR co-localizes with the dentate granule cell marker calbindin in hippocampal neurons. Double-label immunostaining for IRβ (*green*) and the dentate granule cell marker calbindin *(red)* in (A) hippocampal neurons (scale 100μm) and (B) hippocampal cultures (scale 10μm). IR co-localizes with calbindin in WT hippocampal neurons *(merge).*

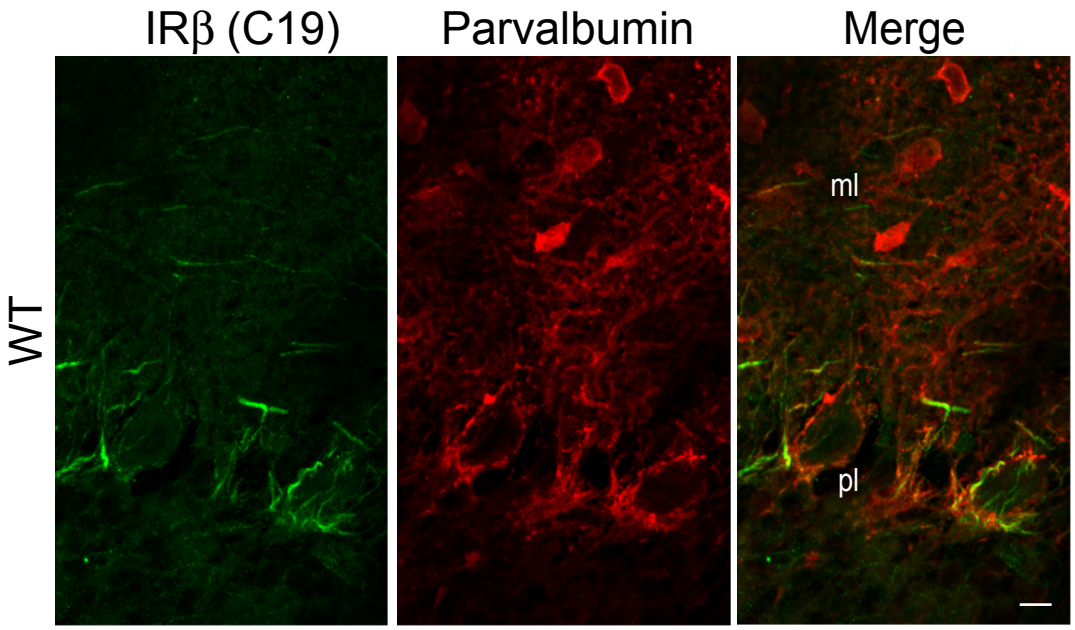

Figure 3.1.4. IR co-localizes with the basket cell marker parvalbumin in the cerebellum. Double-label immunohistochemistry for IRβ (*green*) and the basket cell marker parvalbumin *(red)* in cerebellar sections. IR co-localizes with parvalbumin in WT cerebellar neurons *(merge)*. Molecular layer (ml), Purkinje layer (pl). Scale 10μm.

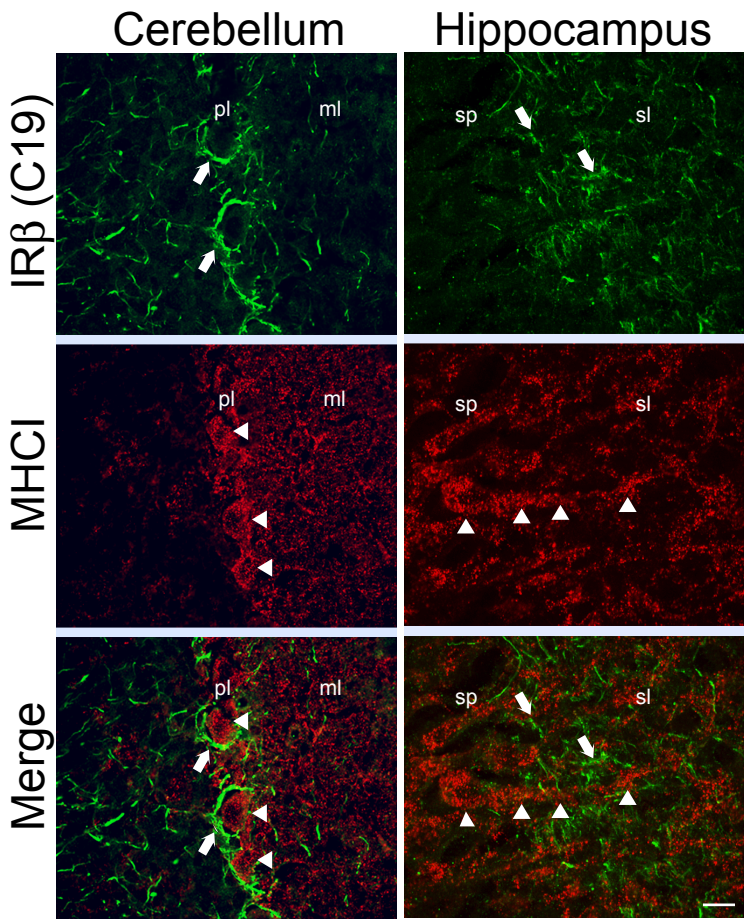

Figure 3.2.1. MHCI and IR are expressed in close apposition. Coronal sections of P30 mouse brain sections immunostained for IRβ (C19, *green*) and MHCI *(red)*. MHCI proteins are expressed in soma and dendrites (arrowheads) in close apposition to IR-positive axons (arrows) in the Purkinje layer (pl) of cerebellum and stratum lucidum (sl) of hippocampus (*merge)*. Molecular layer (ml), stratum pyramidale (sp). Scale 20μm.

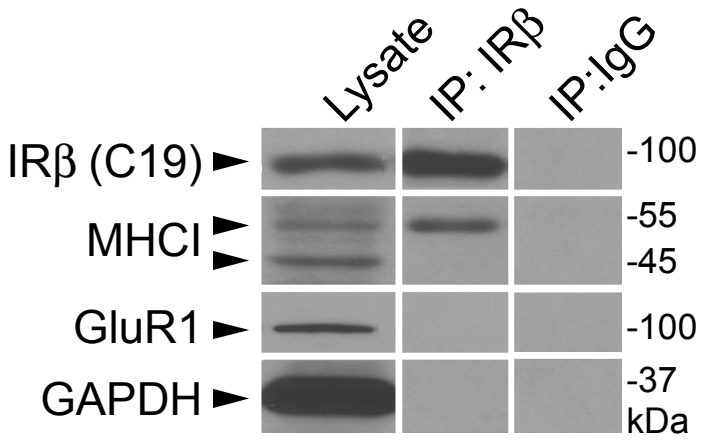

Figure 3.3.1. MHCI and IR co-immunoprecipitate from WT hippocampal lysates. Western blot of IR immunoprecipitated from mouse hippocampal lysates. IR and MHCI proteins are detected in total WT hippocampal lysates. Immunoprecipitation using IRβ (C19) antibodies enriches for IR and selectively co-precipitates MHCI, but not other highly expressed cell surface (GluR1) or intracellular (GAPDH) proteins. Immunoprecipitation with IgG isotype control does not pull down detectable levels of any of the examined proteins.

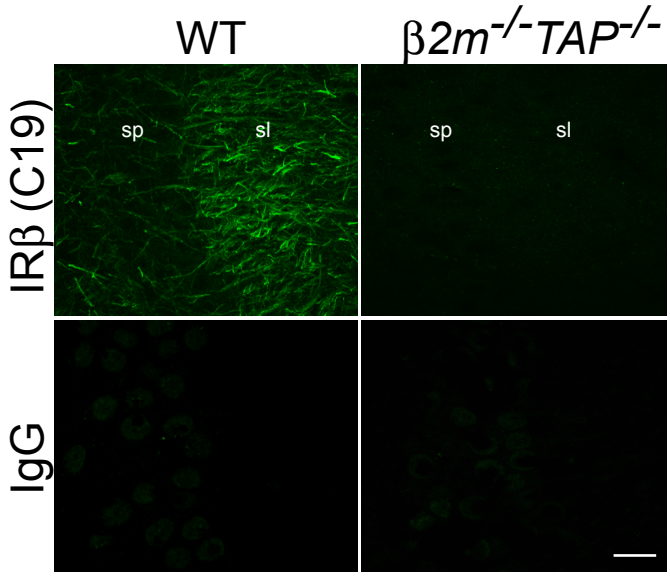

Figure 3.4.1. IR immunostaining is abolished in β*2m*$^{-/-}$*TAP*$^{-/-}$ hippocampal sections. Coronal sections of mouse hippocampus immunostained with IRβ (C19) antibodies or IgG isotype control. IRβ labeling is strong in WT brain but is completely abolished in β*2m*$^{-/-}$*TAP*$^{-/-}$ sections. Stratum pyramidale (sp), stratum lucidum (sl). Scale 20μm.

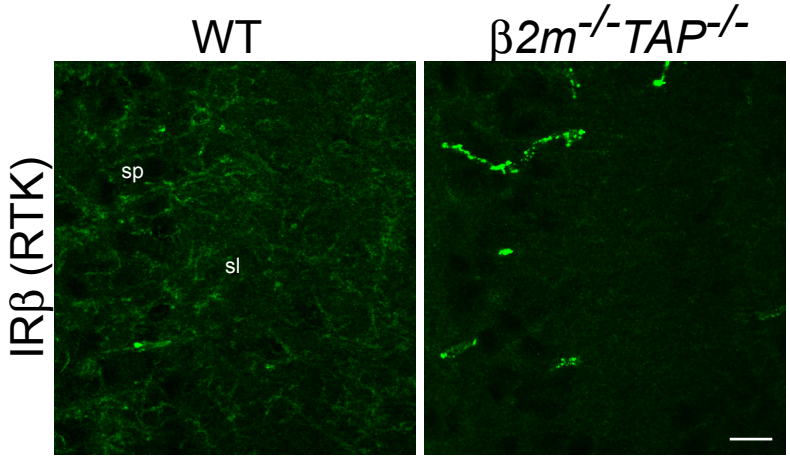

Figure 3.4.2. IR immunostaining is abolished in β*2m*$^{-/-}$*TAP*$^{-/-}$ hippocampal sections using an alternate IR antibody. Coronal sections of mouse hippocampus immunostained with IRβ (RTK) antibodies. IRβ labeling is present in WT brain but is abolished in β*2m*$^{-/-}$*TAP*$^{-/-}$ sections using a different antibody. Stratum pyramidale (sp), stratum lucidum (sl). Scale 20μm.

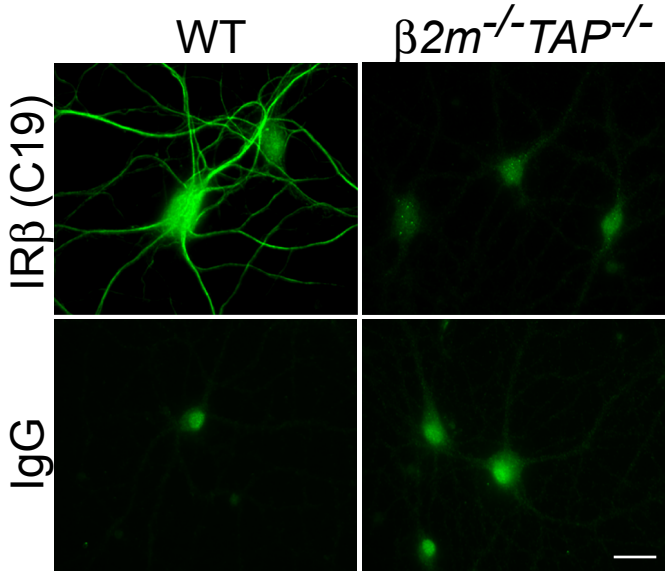

Figure 3.4.3. IR immunostaining is abolished in β*2m*$^{-/-}$*TAP*$^{-/-}$ hippocampal neurons in culture. WT or β*2m*$^{-/-}$*TAP*$^{-/-}$ hippocampal neurons in culture immunostained for IRβ (C19). Strong, specific labeling of WT neurites is completely absent in β*2m*$^{-/-}$*TAP*$^{-/-}$ neurons. Scale 10μm.

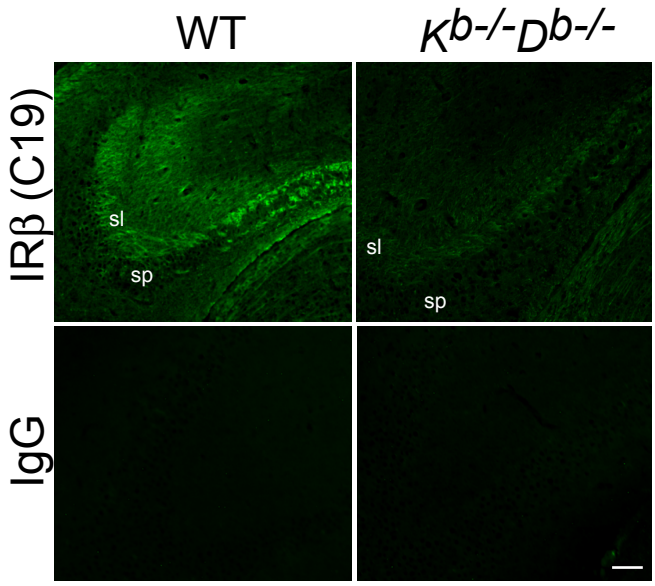

Figure 3.4.4. IR immunostaining is significantly reduced in $K^{b-/-}D^{b-/-}$ hippocampal sections. Coronal sections of mouse brain immunostained with IRβ (C19) antibodies in WT and $K^{b-/-}D^{b-/-}$ hippocampus. IRβ (C19) staining is strong in animals expressing normal levels of MHCI (WT) but is dramatically reduced in mice lacking the classical MHCI proteins *H2-K* and *H2-D* ($K^{b-/-}D^{b-/-}$). Stratum pyramidale (sp), stratum lucidum (sl). Scale 100μm.

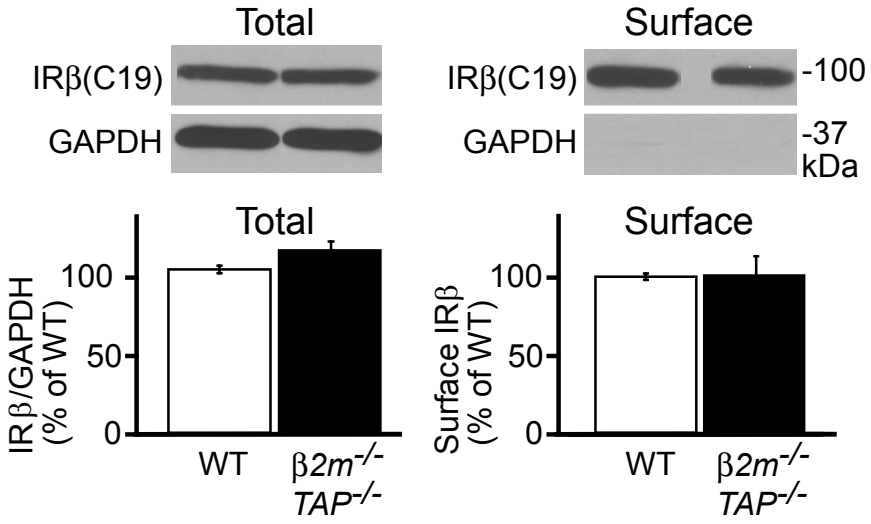

Figure 3.5.1. Total and surface levels or IR protein are normal in β*2m*$^{-/-}$*TAP*$^{-/-}$ hippocampus under denaturing conditions. Western blotting of WT and β*2m*$^{-/-}$ *TAP*$^{-/-}$ total and cell surface fractions probed for IRβ (C19). Quantification: For quantification, total IRβ was normalized to GAPDH, while surface IRβ was normalized to total IRβ levels. Bars represent mean ± SEM (Total: WT 100% ± 2.3%, β*2m*$^{-/-}$*TAP*$^{-/-}$ 111.6% ± 5.5%, n=6 animals; Surface: WT 100% ± 2.0%, β*2m*$^{-/-}$*TAP*$^{-/-}$ 101% ± 12.4%, n=3 animals). Total and surface levels of IR protein are indistinguishable between WT and β*2m*$^{-/-}$*TAP*$^{-/-}$ lysates and show lack of a significant difference using Student's t-test analysis.

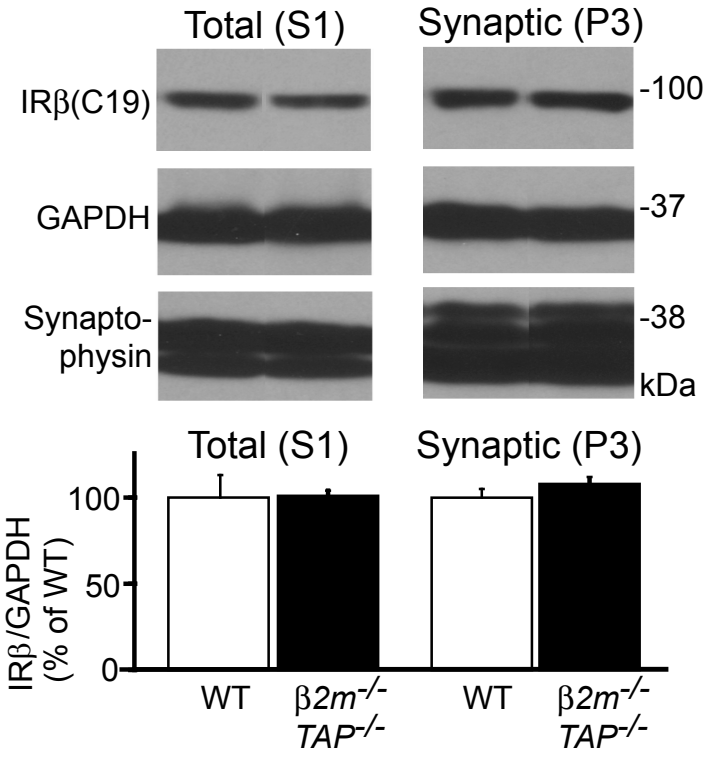

Figure 3.5.2. Synaptic levels of IR protein in $\beta 2m^{-/-}TAP^{-/-}$ hippocampus under denaturing conditions. Total (S1) and synaptic (P3) fractions from microdissected hippocampus probed for IRβ (C19), loading control (GAPDH) and a synaptic protein (synaptophysin). Bars represent mean ± SEM (Total fraction S1; WT 100% ± 13.0%, $\beta 2m^{-/-}TAP^{-/-}$ 100% ± 3.0%, n=6 animals; Synaptic fraction P3; WT 100% ± 5.0%, $\beta 2m^{-/-}TAP^{-/-}$ 108% ± 4.0%, n=6 animals). Synaptic levels of IR protein are indistinguishable between WT and $\beta 2m^{-/-}TAP^{-/-}$ lysates and show lack of a significant difference using a Student's t-test.

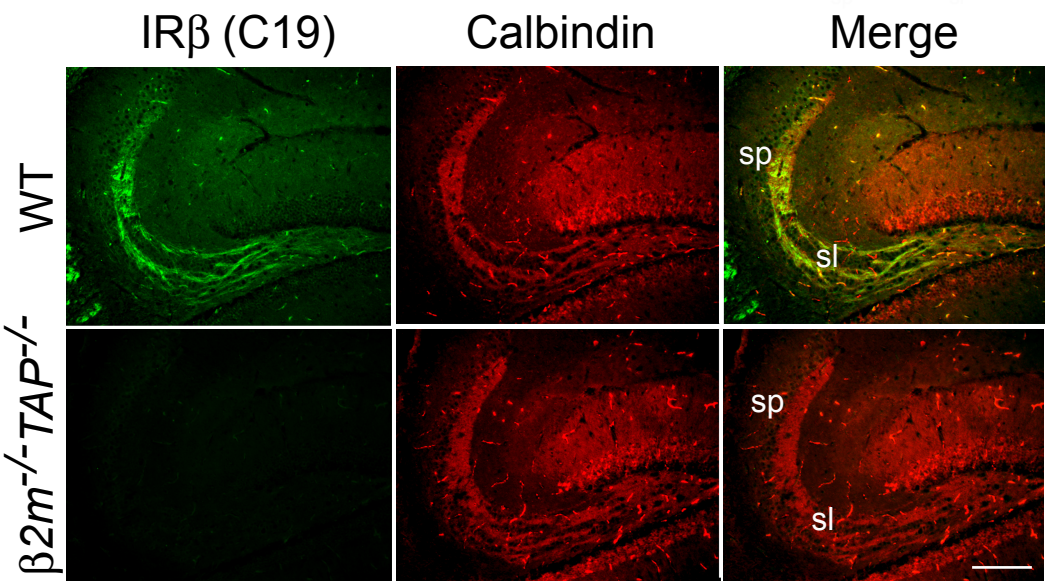

Figure 3.5.3. Dentate granule cell morphology is normal in β*2m*$^{-/-}$*TAP*$^{-/-}$ mice. Double-labeling immunohistochemistry for IRβ (*green*) and the dentate granule cell marker calbindin *(red)*. IRβ and calbindin co-localize in WT neurons. IRβ is absent in β*2m*$^{-/-}$*TAP*$^{-/-}$ hippocampus but calbindin labeling is indistinguishable from WT. Stratum pyramidale (sp), stratum lucidum (sl). Scale 100μm.

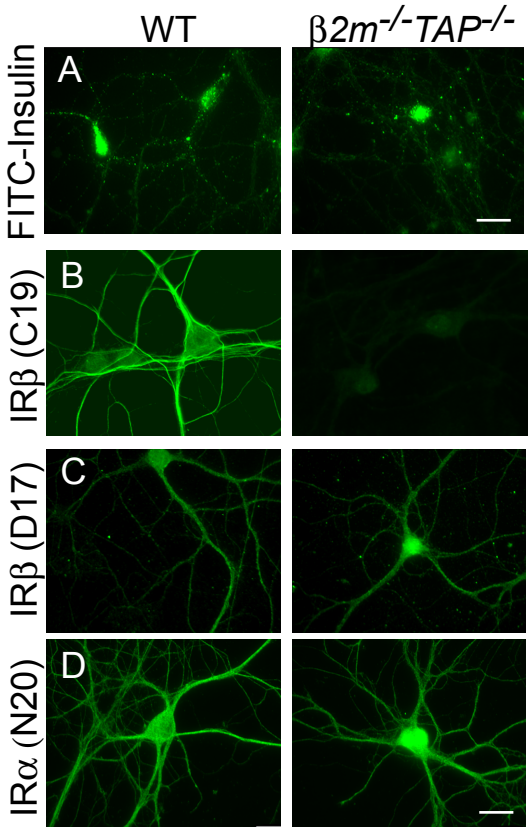

Figure 3.6.1. IR can be detected in β*2m*$^{-/-}$*TAP*$^{-/-}$ hippocampal neurons using reagents directed against distinct epitopes in the and β subunits. (A) Labeling of the cell surface pool of insulin-binding receptors in live, non-permeablized WT and β*2m*$^{-/-}$*TAP*$^{-/-}$ hippocampal neurons using fluorescently-labeled insulin (FITC-insulin). FITC-insulin labeling is qualitatively similar in level and pattern in WT and β*2m*$^{-/-}$*TAP*$^{-/-}$ neurons. Scale 20μm. (B-D) Immunocytochemical staining for total IR protein in permeablized hippocampal neurons using antibodies against the indicated epitopes of IR. Scale 10μm. (B) Labeling with IRβ (C19) is abolished in β*2m*$^{-/-}$*TAP*$^{-/-}$neurons (see also Figures 3.4.1. and 3.4.3.). (C-D) IR protein is detectable in β*2m*$^{-/-}$*TAP*$^{-/-}$neurons when labeled with antibodies against distinct epitopes of the IRβ (D17) or the IRα (N20) subunit.

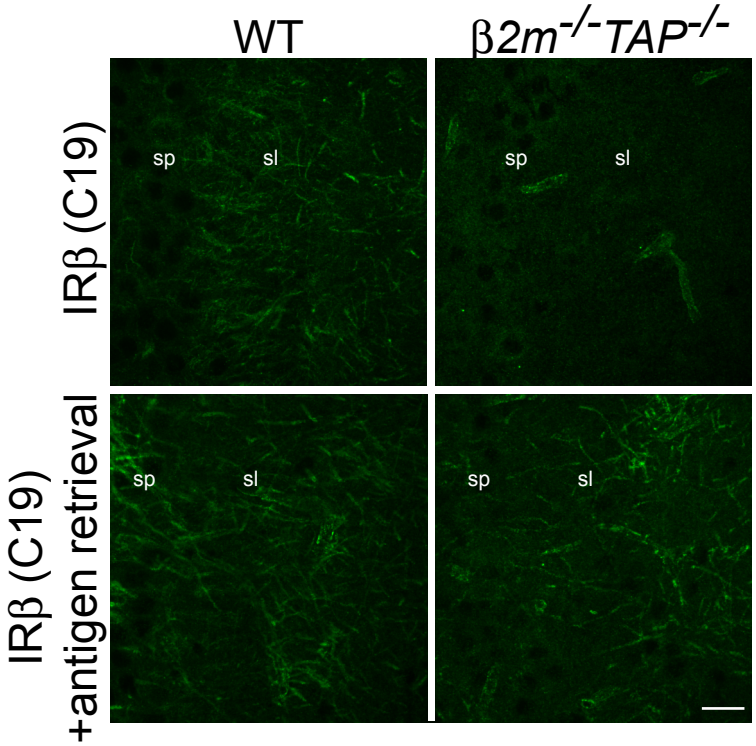

Figure 3.6.2. Immunostaining with IRβ (C19) is recovered in β*2m*$^{-/-}$*TAP*$^{-/-}$ neurons following antigen retrieval. WT and β*2m* $^{-/-}$*TAP*$^{-/-}$ mouse hippocampus immunostained for IRβ (C19) before and after antigen retrieval. IRβ immunolabeling is abolished in β2*m*$^{-/-}$*TAP*$^{-/-}$ brains under normal immunostaining conditions, but can be restored following antigen retrieval techniques to unmask the IRβ (C19) epitope. Scale 25µm.

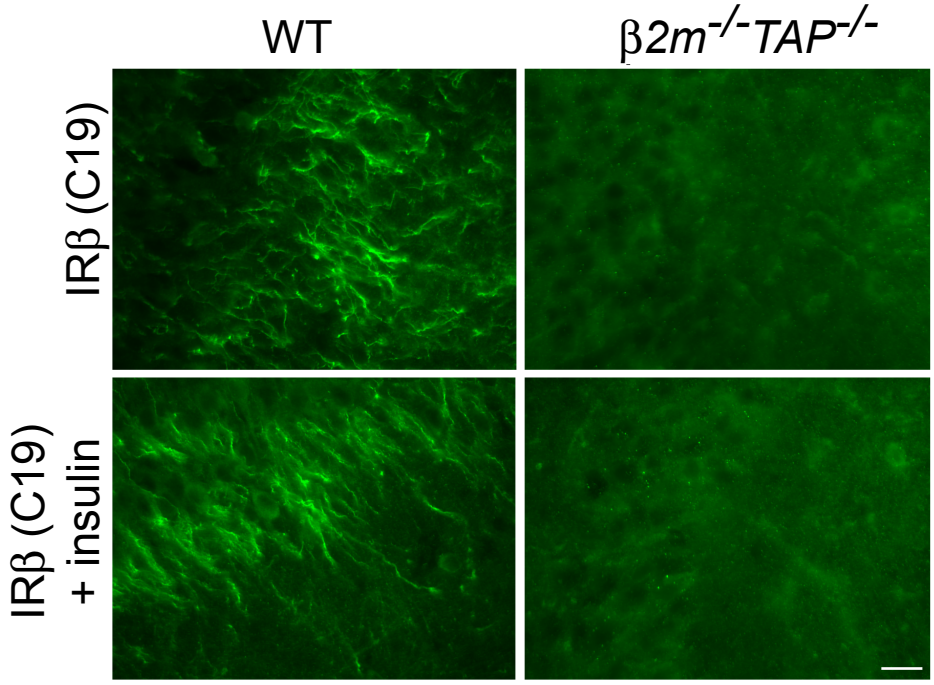

Figure 3.6.3. Loss of IRβ (C19) immunostaining in β*2m*$^{-/-}$*TAP*$^{-/-}$ neurons is not rescued by insulin treatment. Hippocampal slices treated with insulin and immunostained with IRβ (C19) antibodies. Loss of IRβ (C19) labeling is not restored by treatment with the IR ligand insulin. Scale bar 20μm.

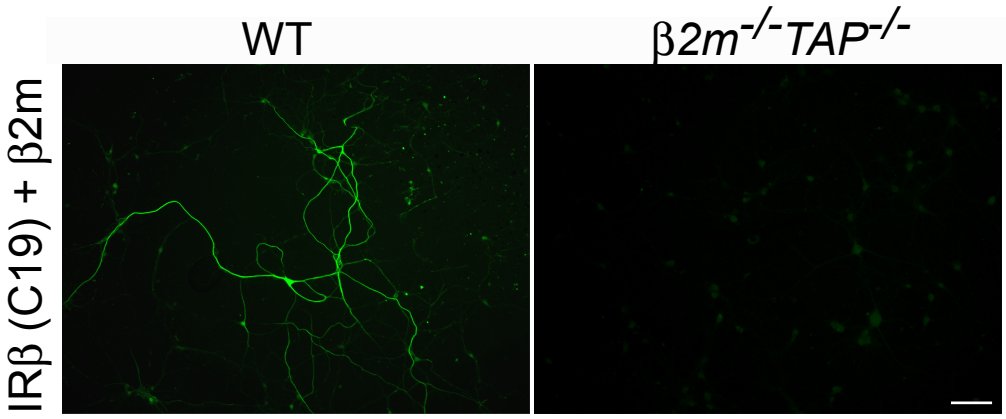

Figure 3.6.4. Loss of IRβ (C19) immunostaining in $\beta 2m^{-/-}TAP^{-/-}$ neurons is not rescued by application of exogenous β_2-microglobulin. Cultured hippocampal neurons treated with β_2-microglobulin (β_2m) and immunostained with IRβ (C19) antibodies. Loss of IRβ (C19) labeling is not restored by treatment with the soluble form of the MHCI light chain β_2 m. Scale bars 50μm.

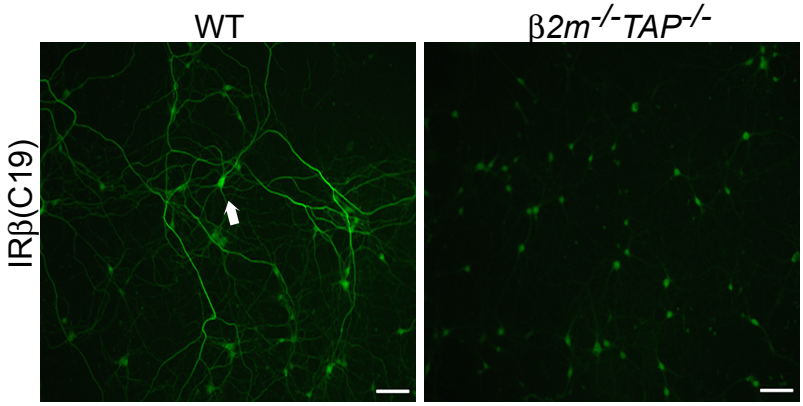

Figure 3.7.1. IRβ (C19) immunolabeling is rescued in β*2m*$^{-/-}$*TAP*$^{-/-}$ neurons co-cultured with WT, MHCI-expressing neurons. Low magnification view of WT or β*2m*$^{-/-}$*TAP*$^{-/-}$ hippocampal neurons in culture immunostained for IRβ (C19). WT cultures contain IR-positive neurons (dentate granule cells) and IR-negative neurons. IR-positive neurons are readily identifiable in WT hippocampal cultures at lower magnifications (arrow). β*2m*$^{-/-}$ *TAP*$^{-/-}$ cultures do not contain any IR-positive neurons. Scale 40μm.

Figure 3.7.2. IRβ (C19) immunolabeling is rescued in *β2m*$^{-/-}$*TAP*$^{-/-}$ neurons co-cultured with WT, MHCI-expressing neurons. (A) Double-labeling immunocytochemistry for IRβ (C19) and GFP in pure WT-GFP or pure *β2m*$^{-/-}$*TAP*$^{-/-}$ hippocampal cultures. Cultures from WT-GFP mice contain many neurons that express both IR and GFP proteins while cultures from *β2m*$^{-/-}$*TAP*$^{-/-}$ mice display neither IR nor GFP protein labeling. Scale 10μm. (B) Double-labeling immunocytochemistry for IRβ (C19) and GFP in WT-GFP and *β2m*$^{-/-}$*TAP*$^{-/-}$ mixed hippocampal co-cultures. Mixed cultures plated with equal numbers of WT-GFP and *β2m*$^{-/-}$*TAP*$^{-/-}$ neurons reveal that IRβ (C19) staining can be rescued in *β2m*$^{-/-}$*TAP*$^{-/-}$ (GFP-negative) neurons (arrows) when cultured in the presence of WT (GFP-positive) neurons (arrowheads). Scale 50μm (40X view) or 20μm (10X view).

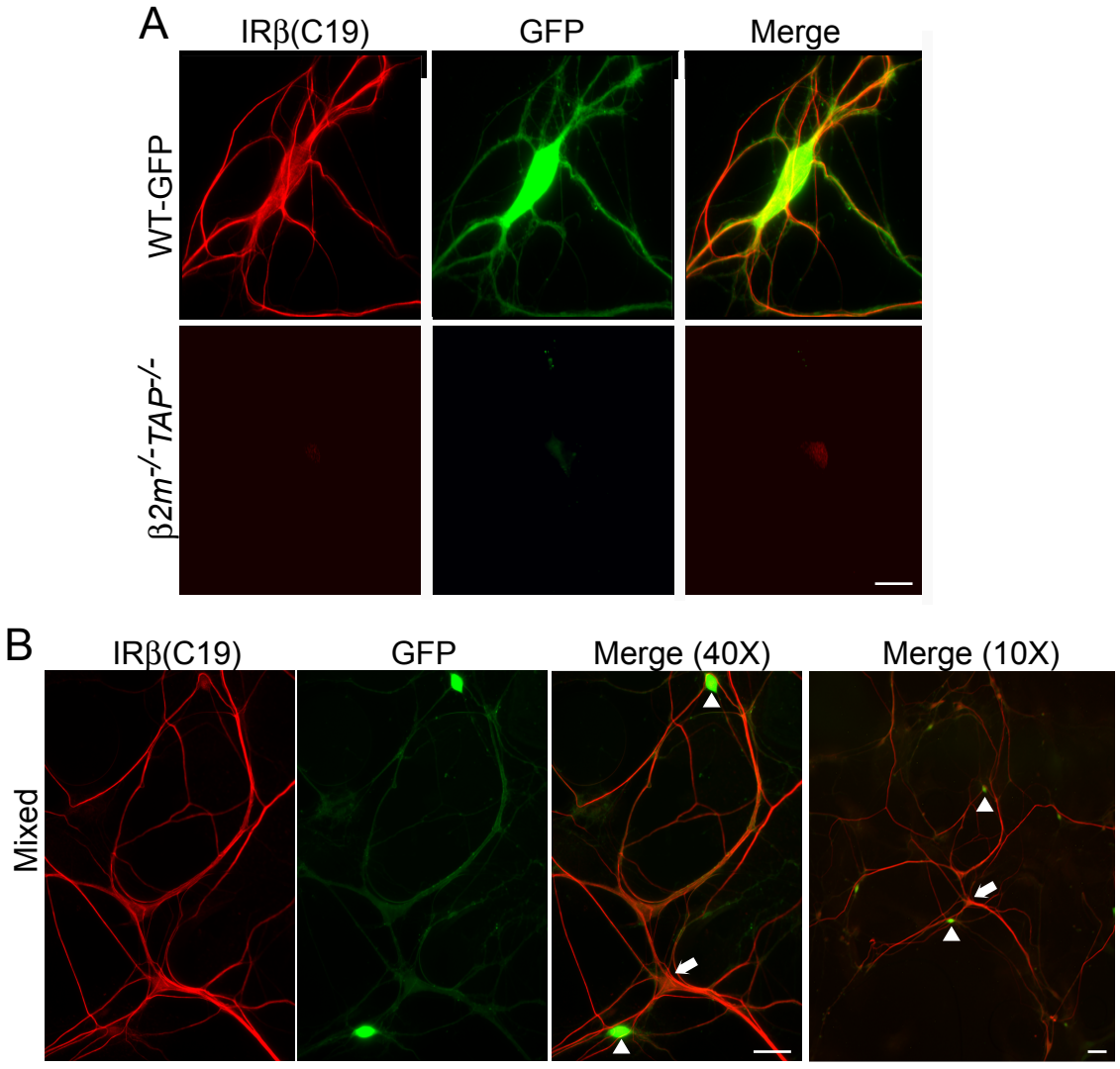
A
IRβ(C19)
GFP
Merge
WT-GFP
β2m-/-TAP-/-
B
IRβ(C19)
GFP
Merge (40X)
Merge (10X)
Mixed

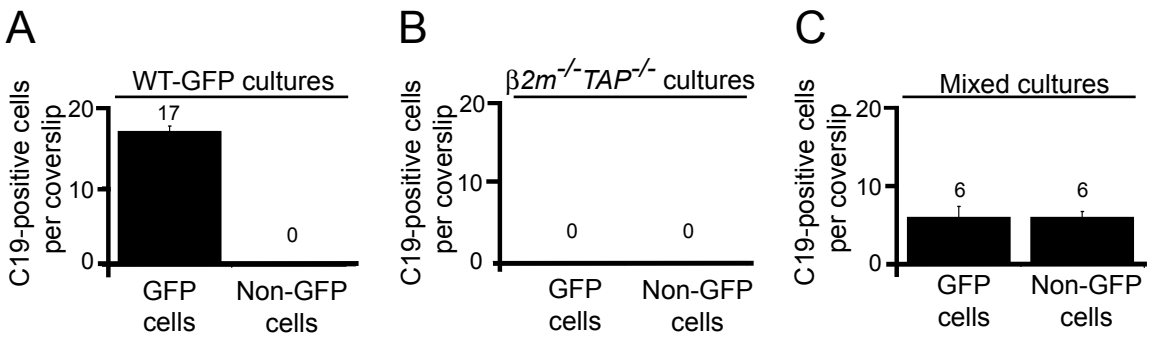

Figure 3.7.3. IRβ (C19) immunolabeling is rescued in β*2m*$^{-/-}$*TAP*$^{-/-}$ neurons co-cultured with WT, MHCI-expressing neurons. (A) Quantification of cells showing IRβ (C19) labeling in WT-GFP cultures. Mature hippocampal cultures from WT-GFP mice contain, on average, 17 C19-positive cells per coverslip. Of note, no WT neurons are GFP-negative. The average number of cells per coverslip is ~300. Bars represent mean ± SEM (GFP cells: 17±0.70; Non-GFP cells: 0, n=3 animals). (B) Quantification of cells showing IRβ (C19) labeling in β*2m*$^{-/-}$*TAP*$^{-/-}$ cultures. Mature hippocampal cultures from β*2m*$^{-/-}$*TAP*$^{-/-}$ mice do not contain any C19-positive cells. Of note, none of the β*2m*$^{-/-}$*TAP*$^{-/-}$ cells are GFP-positive (n=3 animals). (C) Quantification of cells showing IRβ (C19) labeling in WT-GFP/β*2m*$^{-/-}$*TAP*$^{-/-}$ co-cultures. Mature hippocampal cultures plated with equal numbers of WT-GFP and β*2m*$^{-/-}$*TAP*$^{-/-}$ neurons contain two populations of C19-expressing cells: those that are GFP-positive (WT), and those that are GFP-negative (β*2m*$^{-/-}$*TAP*$^{-/-}$). Bars represent mean ± SEM (GFP cells: 6±1.4; Non-GFP cells: 6±0.8 n=3 animals).

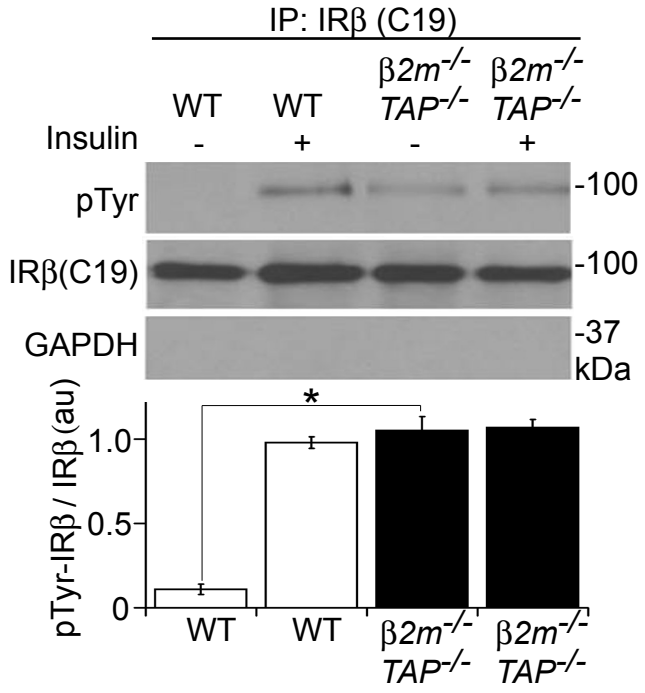

Figure 3.8.1. IR signaling is increased in MHCI-deficient hippocampus. IR immunoprecipitated from WT or β*2m*$^{-/-}$*TAP*$^{-/-}$ hippocampal lysates in the presence or absence of insulin and phosphatase inhibitors, probed for phosphotyrosine (pTyr), IRβ (C19), or a loading control (GAPDH). While total levels of IR are normal, the fraction of neuronal IR that are tyrosine phosphorylated (pTyr-IRβ/IRβ) in the absence of exogenous insulin is significantly elevated in β*2m*$^{-/-}$ *TAP*$^{-/-}$ hippocampus. Treatment with insulin induces a significant increase in tyrosine phosphorylation of IR in WT but not β*2m*$^{-/-}$*TAP*$^{-/-}$ hippocampus. Bars represent mean ± SEM normalized to total IR (WT minus insulin: 0.11±0.03; WT plus insulin: 0.98±0.03; β*2m*$^{-/-}$*TAP*$^{-/-}$ minus insulin: 1.05±0.08, $p<0.01$ as compared to WT minus insulin, Student's t-test; β*2m* $^{-/-}$*TAP*$^{-/-}$ with insulin: 1.07±0.05; n=3 animals per condition).

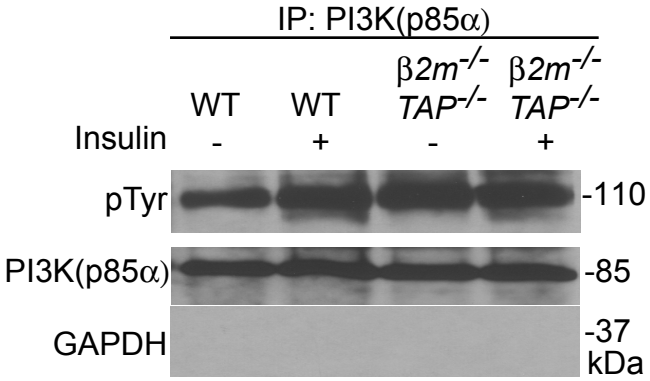

Figure 3.8.2. PI3K signaling is increased in MHCI-deficient hippocampus. The p85α subunit of PI3K immunoprecipitated from WT or β*2m*$^{-/-}$*TAP*$^{-/-}$ hippocampal lysates in the presence or absence of insulin and phosphatase inhibitors, probed for phosphotyrosine (pTyr), PI3K (p85α) or a loading control (GAPDH). While total levels of PI3K (p85α) are normal, the amount of PI3K (p85α) that are tyrosine phosphorylated in the absence of exogenous insulin is elevated in β*2m*$^{-/-}$ *TAP*$^{-/-}$ hippocampus. Treatment with insulin induces a significant increase in tyrosine phosphorylation of PI3K (p85α) in WT but not β*2m*$^{-/-}$*TAP*$^{-/-}$ hippocampus.

Figure 3.9.1. Synapse number is increased in MHCI-deficient hippocampal neurons. (A) Representative high magnification electron micrographs of hippocampal region CA3 from WT, $\beta 2m^{-/-}TAP^{-/-}$ and $K^{b-/-}D^{b-/-}$ mice showing a single synapse. Cross synapse morphology is comparable in WT and knock out mice. Scale 250nm. (B) Representative low magnification electron micrographs of CA3 from WT, $\beta 2m^{-/-}TAP^{-/-}$ and $K^{b-/-}D^{b-/-}$ mice showing multiple synapses (arrowheads). Sclae 150nm. $\beta 2m^{-/-}TAP^{-/-}$ and $K^{b-/-}D^{b-/-}$ mice display a significant increase in synapse density as compared to WT in CA3, where IR is expressed, but not in CA1, where IR is not expressed. Bars represent mean ± SEM (WT: 3.4±0.10 synapses per $10m^2$, n=6 animals; $\beta 2m^{-/-}TAP^{-/-}$: 4.0±0.08, n=6, $p<0.02$; $K^{b-/-}D^{b-/-}$: 4.3±0.03, n=3, $p<0.01$ Student's t-test).

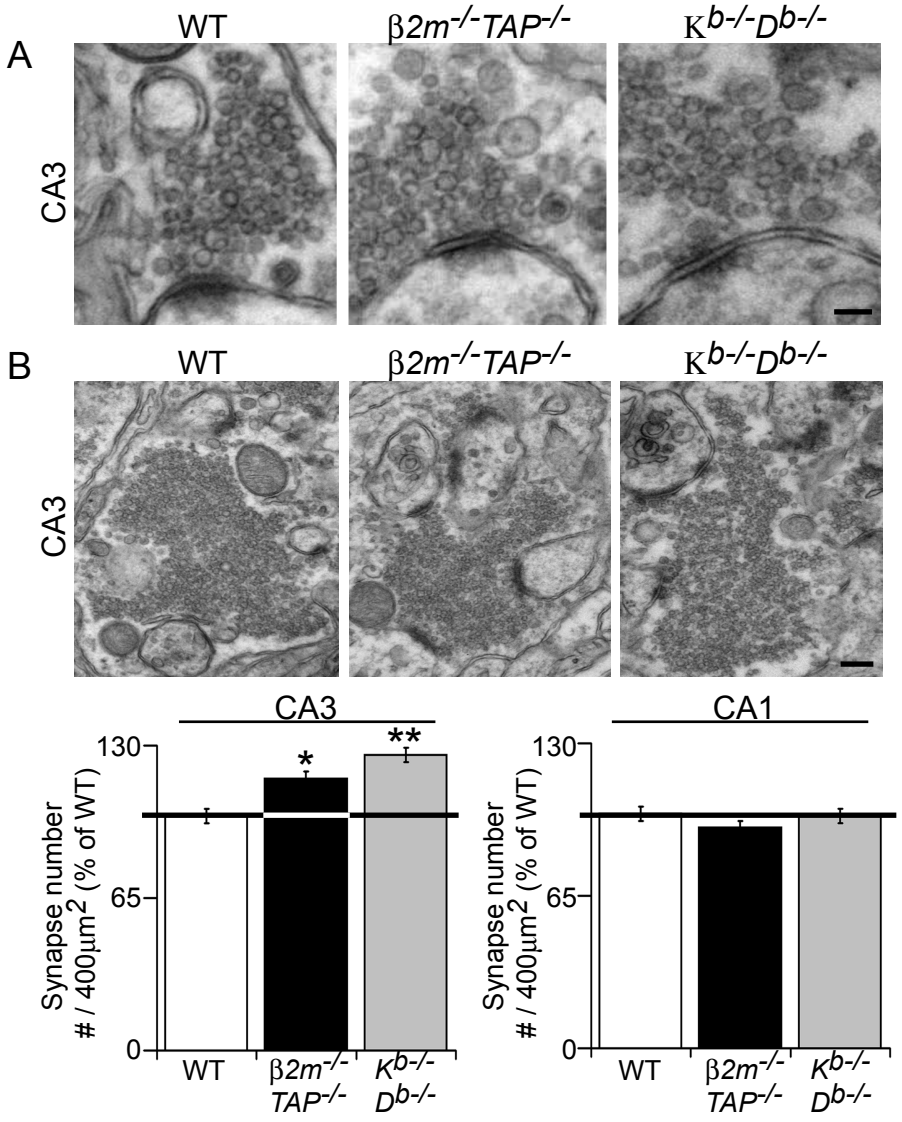
A
WT
β2m-/-TAP-/-
Kb-/-Db-/-
CA3
B
WT
β2m-/-TAP-/-
Kb-/-Db-/-
CA3
CA3
CA1
Synapse number
/ 400μm2 (% of WT)
130
65
0
*
**
WT
β2m-/-
TAP-/-
Kb-/-
Db-/-

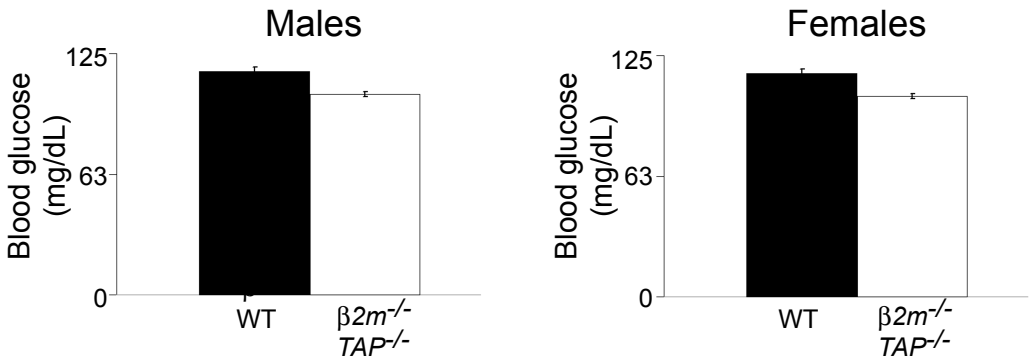

Figure 3.10.1. Fasted blood glucose levels in WT and $\beta 2m^{-/-}TAP^{-/-}$ mice. $\beta 2m^{-/-}TAP^{-/-}$ mice have normal blood glucose levels after 24 hours of fasting. Bars represent mean±SEM (WT males: 115.6±2.5mg/dL, n=12 animals; $\beta 2m^{-/-}TAP^{-/-}$ males: 103.9±1.3, n=19; WT females: 96.9±2.5, n=8, $\beta 2m^{-/-}TAP^{-/-}$ females: 85±1.6, n=19. Student's t-test shows no significant difference).

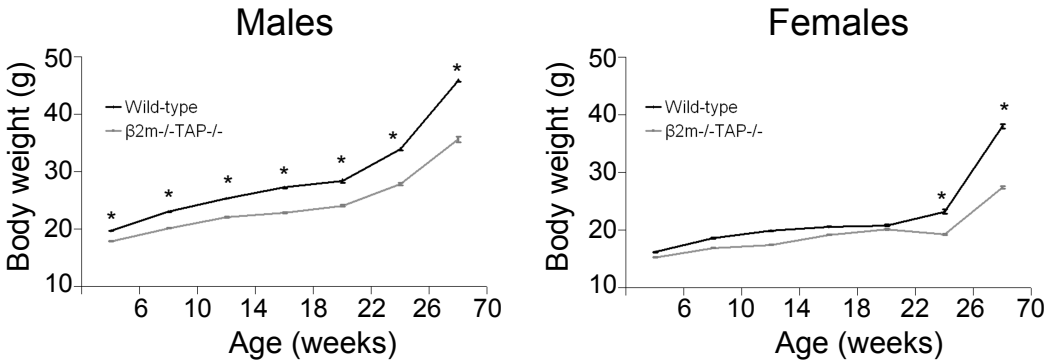

Figure 3.11.1. Body weight measurements in WT and β2m$^{-/-}$*TAP*$^{-/-}$ mice from 6-70 weeks of age. Male β2*m*$^{-/-}$*TAP*$^{-/-}$ mice on a regular chow diet weighed significantly less than controls at all ages, while female β2m$^{-/-}$*TAP*$^{-/-}$ mice weighed significantly less than controls starting at 26 weeks if age. Bars represent mean±SEM (n>10 mice for each genotype and gender, $p<0.0001$ Student's t-test).

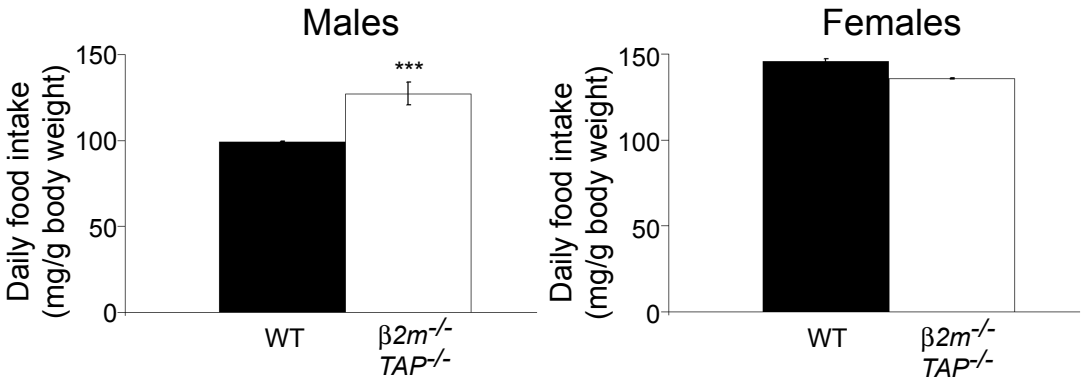

Figure 3.11.2. Food intake measurements normalized to body weight in WT and $\beta 2m^{-/-}TAP^{-/-}$ mice at 20 weeks of age. $\beta 2m^{-/-}TAP^{-/-}$ male mice eat significantly more than controls relative to their body weight, while $\beta 2m^{-/-}TAP^{-/-}$ female mice do not have altered normalized food intake. Bars represent mean±SEM (WT males: 99.1±0.6 mg/g body weight, n=15 animals; $\beta 2m^{-/-}TAP^{-/-}$ males: 127.2±6.6, n=15, $p<0.0001$ Student's t-test; WT females: 145.7±1.3, n=19, $\beta 2m^{-/-}TAP^{-/-}$ females: 135.6±0.36, n=14).

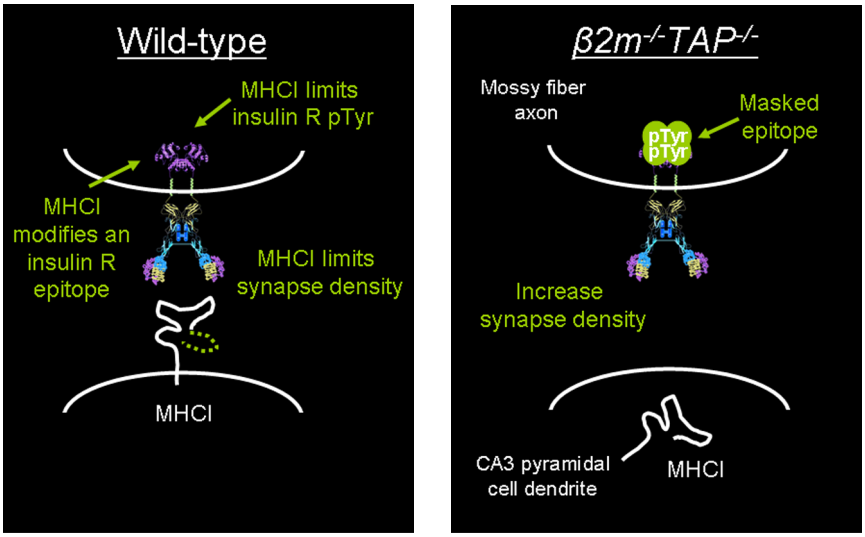

Figure 3.12.1. Summary of IR signaling in WT β*2m*$^{-/-}$*TAP*$^{-/-}$ hippocampal neurons. In WT neurons, endogenous MHCI acts to limit the signaling of IR and additionally limits synapse density, a process that is dependent on normally functioning IR. In β*2m*$^{-/-}$*TAP*$^{-/-}$ neurons, loss of cell surface MHCI leads to a masking of a key cytoplasmic domain of IR, an increase in the basal activation of IR and an increase in synapse density specifically in regions where IR are expressed. This model suggests a mechanism whereby MHCI modulates the tyrosine phosphorylated cytoplasmic tails of IR to regulate synaptic density in the hippocampus.

REFERENCES

Abbott, M. A., Wells, D. G., and Fallon, J. R. (1999). The insulin receptor tyrosine kinase substrate p58/53 and the insulin receptor are components of CNS synapses. J Neurosci *19*, 7300-7308.

Ahmadian, G., Ju, W., Liu, L., Wyszynski, M., Lee, S. H., Dunah, A. W., Taghibiglou, C., Wang, Y., Lu, J., Wong, T. P., *et al.* (2004). Tyrosine phosphorylation of GluR2 is required for insulin-stimulated AMPA receptor endocytosis and LTD. Embo J *23*, 1040-1050.

Assa-Kunik, E., Fishman, D., Kellman-Pressman, S., Tsory, S., Elhyany, S., Baharir, O., and Segal, S. (2003). Alterations in the expression of MHC class I glycoproteins by B16BL6 melanoma cells modulate insulin receptor-regulated signal transduction and augment [correction of augments] resistance to apoptosis. J Immunol *171*, 2945-2952.

Baudler, S., Baumgartl, J., Hampel, B., Buch, T., Waisman, A., Snapper, C. M., Krone, W., and Bruning, J. C. (2005). Insulin-like growth factor-1 controls type 2 T cell-independent B cell response. J Immunol *174*, 5516-5525.

Beattie, E. C., Carroll, R. C., Yu, X., Morishita, W., Yasuda, H., von Zastrow, M., and Malenka, R. C. (2000). Regulation of AMPA receptor endocytosis by a signaling mechanism shared with LTD. Nat Neurosci *3*, 1291-1300.

Benedict, L., Nelson, C. A., Schunk, E., Sullwold, K., and Seaquist, E. R. (2006). Effect of insulin on the brain activity obtained during visual and memory tasks in healthy human subjects. Neuroendocrinology *83*, 20-26.

Bennett, M. J., Lebron, J. A., and Bjorkman, P. J. (2000). Crystal structure of the hereditary haemochromatosis protein HFE complexed with transferrin receptor. Nature *403*, 46-53.

Boyington, J. C., and Sun, P. D. (2002). A structural perspective on MHC class I recognition by killer cell immunoglobulin-like receptors. Mol Immunol *38*, 1007-1021.

Bruning, J. C., Gautam, D., Burks, D. J., Gillette, J., Schubert, M., Orban, P. C., Klein, R., Krone, W., Muller-Wieland, D., and Kahn, C. R. (2000). Role of brain insulin receptor in control of body weight and reproduction. Science *289*, 2122-2125.

Chiu, S. L., Chen, C. M., and Cline, H. T. (2008). Insulin receptor signaling regulates synapse number, dendritic plasticity, and circuit function in vivo. Neuron *58*, 708-719.

Chvatchko, Y., Van Obberghen, E., Kiger, N., and Fehlmann, M. (1983).

Immunoprecipitation of insulin receptors by antibodies against Class 1 antigens of the murine H-2 major histocompatibility complex. FEBS Lett *163*, 207-211.

De Meyts, P., and Whittaker, J. (2002). Structural biology of insulin and IGF1 receptors: implications for drug design. Nat Rev Drug Discov *1*, 769-783.

Due, C., Simonsen, M., and Olsson, L. (1986). The major histocompatibility complex class I heavy chain as a structural subunit of the human cell membrane insulin receptor: implications for the range of biological functions of histocompatibility antigens. Proc Natl Acad Sci U S A *83*, 6007-6011.

Edidin, M., and Reiland, J. (1990). Dynamic measurements of the associations between class I MHC antigens and insulin receptors. Mol Immunol *27*, 1313-1317.

Entingh-Pearsall, A., and Kahn, C. R. (2004). Differential roles of the insulin and insulin-like growth factor-I (IGF-I) receptors in response to insulin and IGF-I. J Biol Chem *279*, 38016-38024.

Fisher, S. J., Bruning, J. C., Lannon, S., and Kahn, C. R. (2005). Insulin signaling in the central nervous system is critical for the normal sympathoadrenal response to hypoglycemia. Diabetes *54*, 1447-1451.

Fleming, R. E., Holden, C. C., Tomatsu, S., Waheed, A., Brunt, E. M., Britton, R. S., Bacon, B. R., Roopenian, D. C., and Sly, W. S. (2001). Mouse strain differences determine severity of iron accumulation in Hfe knockout model of hereditary hemochromatosis. Proc Natl Acad Sci U S A *98*, 2707-2711.

Goddard, C. A., Butts, D. A., and Shatz, C. J. (2007). Regulation of CNS synapses by neuronal MHC class I. Proc Natl Acad Sci U S A *104*, 6828-6833.

Hansen, T., Stagsted, J., Pedersen, L., Roth, R. A., Goldstein, A., and Olsson, L. (1989). Inhibition of insulin receptor phosphorylation by peptides derived from major histocompatibility complex class I antigens. Proc Natl Acad Sci U S A *86*, 3123-3126.

Havrankova, J., Roth, J., and Brownstein, M. (1978). Insulin receptors are widely distributed in the central nervous system of the rat. Nature *272*, 827-829.

Held, W., and Mariuzza, R. A. (2008). Cis interactions of immunoreceptors with MHC and non-MHC ligands. Nat Rev Immunol *8*, 269-278.

Horton, R., Wilming, L., Rand, V., Lovering, R. C., Bruford, E. A., Khodiyar, V. K., Lush, M. J., Povey, S., Talbot, C. C., Jr., Wright, M. W., *et al.* (2004). Gene map of the extended human MHC. Nat Rev Genet *5*, 889-899.

Huang, C. C., You, J. L., Lee, C. C., and Hsu, K. S. (2003). Insulin induces a novel form of postsynaptic mossy fiber long-term depression in the hippocampus. Mol Cell Neurosci *24*, 831-841.

Hubbard, S. R., Wei, L., Ellis, L., and Hendrickson, W. A. (1994). Crystal structure of the tyrosine kinase domain of the human insulin receptor. Nature *372*, 746-754.

Huh, G. S., Boulanger, L. M., Du, H., Riquelme, P. A., Brotz, T. M., and Shatz, C. J. (2000). Functional requirement for class I MHC in CNS development and plasticity. Science *290*, 2155-2159.

Kar, S., Chabot, J. G., and Quirion, R. (1993). Quantitative autoradiographic localization of [125I]insulin-like growth factor I, [125I]insulin-like growth factor II, and [125I]insulin receptor binding sites in developing and adult rat brain. J Comp Neurol *333*, 375-397.

Kar, S., Seto, D., Dore, S., Chabot, J. G., and Quirion, R. (1997). Systemic administration of kainic acid induces selective time dependent decrease in [125I]insulin-like growth factor I, [125I]insulin-like growth factor II and [125I]insulin receptor binding sites in adult rat hippocampal formation. Neuroscience *80*, 1041-1055.

Lamothe, B., Bucchini, D., Jami, J., and Joshi, R. L. (1995). Interaction of p85 subunit of PI 3-kinase with insulin and IGF-1 receptors analysed by using the two-hybrid system. FEBS Lett *373*, 51-55.

Letellier, M., Willson, M. L., Gautheron, V., Mariani, J., and Lohof, A. M. (2008). Normal adult climbing fiber monoinnervation of cerebellar Purkinje cells in mice lacking MHC class I molecules. Dev Neurobiol *68*, 997-1006.

Lidman, O., Olsson, T., and Piehl, F. (1999). Expression of nonclassical MHC class I (RT1-U) in certain neuronal populations of the central nervous system. Eur J Neurosci *11*, 4468-4472.

Liegler, T., Szollosi, J., Hyun, W., and Goodenow, R. S. (1991). Proximity measurements between H-2 antigens and the insulin receptor by fluorescence energy transfer: evidence that a close association does not influence insulin binding. Proc Natl Acad Sci U S A *88*, 6755-6759.

Lin, J. W., Ju, W., Foster, K., Lee, S. H., Ahmadian, G., Wyszynski, M., Wang, Y. T., and Sheng, M. (2000). Distinct molecular mechanisms and divergent endocytotic pathways of AMPA receptor internalization. Nat Neurosci *3*, 1282-1290.

Linda, H., Hammarberg, H., Piehl, F., Khademi, M., and Olsson, T. (1999). Expression of MHC class I heavy chain and beta2-microglobulin in rat brainstem motoneurons and nigral dopaminergic neurons. J Neuroimmunol *101*, 76-86.

Ljunggren, H. G., Van Kaer, L., Sabatine, M. S., Auchincloss, H., Jr., Tonegawa, S., and Ploegh, H. L. (1995). MHC class I expression and CD8+ T cell development in TAP1/beta 2-microglobulin double mutant mice. Int Immunol *7*, 975-984.

Man, H. Y., Lin, J. W., Ju, W. H., Ahmadian, G., Liu, L., Becker, L. E., Sheng, M., and Wang, Y. T. (2000). Regulation of AMPA receptor-mediated synaptic transmission by clathrin-dependent receptor internalization. Neuron *25*, 649-662.

McConnell, M. J., Huang, Y. H., Datwani, A., and Shatz, C. J. (2009). H2-Kb and H2-Db regulate cerebellar long-term depression and limit motor learning. Proc Natl Acad Sci U S A.

McInnes, C., and Sykes, B. D. (1997). Growth factor receptors: structure, mechanism, and drug discovery. Biopolymers *43*, 339-366.

Milner, C. M., and Campbell, R. D. (1992). Genes, genes and more genes in the human major histocompatibility complex. Bioessays *14*, 565-571.

Monaco, J. J. (1992). A molecular model of MHC class-I-restricted antigen processing. Immunol Today *13*, 173-179.

Neefjes, J. J., and Momburg, F. (1993). Cell biology of antigen presentation. Curr Opin Immunol *5*, 27-34.

Ojcius, D. M., Delarbre, C., Kourilsky, P., and Gachelin, G. (2002). MHC and MHC-related proteins as pleiotropic signal molecules. Faseb J *16*, 202-206.

Okabe, M., Ikawa, M., Kominami, K., Nakanishi, T., and Nishimune, Y. (1997). 'Green mice' as a source of ubiquitous green cells. FEBS Lett *407*, 313-319.

Oliveira, A. L., Thams, S., Lidman, O., Piehl, F., Hokfelt, T., Karre, K., Linda, H., and Cullheim, S. (2004). A role for MHC class I molecules in synaptic plasticity and regeneration of neurons after axotomy. Proc Natl Acad Sci U S A *101*, 17843-17848.

Olsson, L., Goldstein, A., and Stagsted, J. (1994). Regulation of receptor internalization by the major histocompatibility complex class I molecule. Proc Natl Acad Sci U S A *91*, 9086-9090.

Passafaro, M., Piech, V., and Sheng, M. (2001). Subunit-specific temporal and spatial patterns of AMPA receptor exocytosis in hippocampal neurons. Nat Neurosci *4*, 917-926.

Phillips, M. L., Moule, M. L., Delovitch, T. L., and Yip, C. C. (1986). Class I histocompatibility antigens and insulin receptors: evidence for interactions. Proc Natl Acad Sci U S A *83*, 3474-3478.

Plum, L., Schubert, M., and Bruning, J. C. (2005). The role of insulin receptor signaling in the brain. Trends Endocrinol Metab *16*, 59-65.

Polleux, F., and Ghosh, A. (2002). The slice overlay assay: a versatile tool to study the influence of extracellular signals on neuronal development. Sci STKE *2002*, PL9.

Rammensee, H. G., Falk, K., and Rotzschke, O. (1993). MHC molecules as peptide receptors. Curr Opin Immunol *5*, 35-44.

Rhodes, D. A., and Trowsdale, J. (1999). Genetics and molecular genetics of the MHC. Rev Immunogenet *1*, 21-31.

Russell, S. J., and Kahn, C. R. (2007). Endocrine regulation of ageing. Nat Rev Mol Cell Biol *8*, 681-691.

Samson, M., Cousin, J. L., and Fehlmann, M. (1986). Cross-linking of insulin receptors to MHC antigens in human B lymphocytes: evidence for selective molecular interactions. J Immunol *137*, 2293-2298.

Schott, E., Bonasio, R., and Ploegh, H. L. (2003). Elimination in vivo of developing T cells by natural killer cells. J Exp Med *198*, 1213-1224.

Schulingkamp, R. J., Pagano, T. C., Hung, D., and Raffa, R. B. (2000). Insulin receptors and insulin action in the brain: review and clinical implications. Neurosci Biobehav Rev *24*, 855-872.

Shawar, S. M., Vyas, J. M., Rodgers, J. R., and Rich, R. R. (1994). Antigen presentation by major histocompatibility complex class I-B molecules. Annu Rev Immunol *12*, 839-880.

Shi, S. R., Cote, R. J., and Taylor, C. R. (2001). Antigen retrieval techniques: current perspectives. J Histochem Cytochem *49*, 931-937.

Shpakov, A. O., and Pertseva, M. N. (2000). Structural and functional characterization of insulin receptor substrate proteins and the molecular mechanisms of their interaction with insulin superfamily tyrosine kinase receptors and effector proteins. Membr Cell Biol *13*, 455-484.

Skeberdis, V. A., Lan, J., Zheng, X., Zukin, R. S., and Bennett, M. V. (2001). Insulin promotes rapid delivery of N-methyl-D- aspartate receptors to the cell surface by exocytosis. Proc Natl Acad Sci U S A *98*, 3561-3566.

Sproule, T. J., Jazwinska, E. C., Britton, R. S., Bacon, B. R., Fleming, R. E., Sly, W. S., and Roopenian, D. C. (2001). Naturally variant autosomal and sex-linked loci determine

the severity of iron overload in beta 2-microglobulin-deficient mice. Proc Natl Acad Sci U S A *98*, 5170-5174.

Stagsted, J., Mapelli, C., Meyers, C., Matthews, B. W., Anfinsen, C. B., Goldstein, A., and Olsson, L. (1993). Amino acid residues essential for biological activity of a peptide derived from a major histocompatibility complex class I antigen. Proc Natl Acad Sci U S A *90*, 7686-7690.

Stagsted, J., Reaven, G. M., Hansen, T., Goldstein, A., and Olsson, L. (1990). Regulation of insulin receptor functions by a peptide derived from a major histocompatibility complex class I antigen. Cell *62*, 297-307.

Syken, J., Grandpre, T., Kanold, P. O., and Shatz, C. J. (2006). PirB restricts ocular-dominance plasticity in visual cortex. Science *313*, 1795-1800.

Tatar, M., Kopelman, A., Epstein, D., Tu, M. P., Yin, C. M., and Garofalo, R. S. (2001). A mutant Drosophila insulin receptor homolog that extends life-span and impairs neuroendocrine function. Science *292*, 107-110.

Tomioka, M., Adachi, T., Suzuki, H., Kunitomo, H., Schafer, W. R., and Iino, Y. (2006). The insulin/PI 3-kinase pathway regulates salt chemotaxis learning in Caenorhabditis elegans. Neuron *51*, 613-625.

Tomlinson, D. R., and Gardiner, N. J. (2008). Glucose neurotoxicity. Nat Rev Neurosci *9*, 36-45.

Ullrich, A., and Schlessinger, J. (1990). Signal transduction by receptors with tyrosine kinase activity. Cell *61*, 203-212.

Unger, J., McNeill, T. H., Moxley, R. T., 3rd, White, M., Moss, A., and Livingston, J. N. (1989). Distribution of insulin receptor-like immunoreactivity in the rat forebrain. Neuroscience *31*, 143-157.

van der Heide, L. P., Kamal, A., Artola, A., Gispen, W. H., and Ramakers, G. M. (2005). Insulin modulates hippocampal activity-dependent synaptic plasticity in a N-methyl-d-aspartate receptor and phosphatidyl-inositol-3-kinase-dependent manner. J Neurochem *94*, 1158-1166.

Van Horn, D. J., Myers, M. G., Jr., and Backer, J. M. (1994). Direct activation of the phosphatidylinositol 3'-kinase by the insulin receptor. J Biol Chem *269*, 29-32.

Van Kaer, L., Ashton-Rickardt, P. G., Ploegh, H. L., and Tonegawa, S. (1992). TAP1 mutant mice are deficient in antigen presentation, surface class I molecules, and CD4-8+ T cells. Cell *71*, 1205-1214.

Van Obberghen, E., Ballotti, R., Gazzano, H., Fehlmann, M., Rossi, B., Gammeltoft, S., Debant, A., Le Marchand-Brustel, Y., and Kowalski, A. (1985). The insulin receptor kinase. Biochimie *67*, 1119-1124.

Verland, S., Simonsen, M., Gammeltoft, S., Allen, H., Flavell, R. A., and Olsson, L. (1989). Specific molecular interaction between the insulin receptor and a D product of MHC class I. J Immunol *143*, 945-951.

Vugmeyster, Y., Glas, R., Perarnau, B., Lemonnier, F. A., Eisen, H., and Ploegh, H. (1998). Major histocompatibility complex (MHC) class I KbDb -/- deficient mice possess functional CD8+ T cells and natural killer cells. Proc Natl Acad Sci U S A *95*, 12492-12497.

Wan, Q., Xiong, Z. G., Man, H. Y., Ackerley, C. A., Braunton, J., Lu, W. Y., Becker, L. E., MacDonald, J. F., and Wang, Y. T. (1997). Recruitment of functional GABA(A) receptors to postsynaptic domains by insulin. Nature *388*, 686-690.

Ward, C. W., and Lawrence, M. C. (2009). Ligand-induced activation of the insulin receptor: a multi-step process involving structural changes in both the ligand and the receptor. Bioessays *31*, 422-434.

Weiss, E. H., Golden, L., Fahrner, K., Mellor, A. L., Devlin, J. J., Bullman, H., Tiddens, H., Bud, H., and Flavell, R. A. (1984). Organization and evolution of the class I gene family in the major histocompatibility complex of the C57BL/10 mouse. Nature *310*, 650-655.

White, M. F., and Kahn, C. R. (1994). The insulin signaling system. J Biol Chem *269*, 1-4.

Zhao, W., Chen, H., Xu, H., Moore, E., Meiri, N., Quon, M. J., and Alkon, D. L. (1999). Brain insulin receptors and spatial memory. Correlated changes in gene expression, tyrosine phosphorylation, and signaling molecules in the hippocampus of water maze trained rats. J Biol Chem *274*, 34893-34902.

Zhong, J., Zhang, T., and Bloch, L. M. (2006). Dendritic mRNAs encode diversified functionalities in hippocampal pyramidal neurons. BMC Neurosci *7*, 17.

Zijlstra, M., Li, E., Sajjadi, F., Subramani, S., and Jaenisch, R. (1989). Germ-line transmission of a disrupted beta 2-microglobulin gene produced by homologous recombination in embryonic stem cells. Nature *342*, 435-438.